HHS Public Access

Author manuscript

Mol Microbiol. Author manuscript; available in PMC 2020 April 01.

Published in final edited form as:

Mol Microbiol. 2019 April ; 111(4): 1074–1092. doi:10.1111/mmi.14212.

Agrobacterium tumefaciens divisome proteins regulate the transition from polar growth to cell division

Matthew Howell[1], **Alena Aliashkevich**[2], **Kousik Sundararajan**[3,*], **Jeremy J. Daniel**[1], **Patrick J. Lariviere**[3], **Erin D. Goley**[3], **Felipe Cava**[2], and **Pamela J.B. Brown**[1,#]

[1]Division of Biological Sciences, University of Missouri, Columbia, MO, 65203

[2]Department of Molecular Biology. Laboratory for Molecular Infection Medicine Sweden (MIMS), Umeå Centre for Microbial Research, Umeå University, Umeå, Sweden

[3]Department of Biological Chemistry, Johns Hopkins University School of Medicine, Baltimore, MD 21205

Summary

The mechanisms that restrict peptidoglycan biosynthesis to the pole during elongation and re-direct peptidoglycan biosynthesis to mid-cell during cell division in polar-growing Alphaproteobacteria are largely unknown. Here, we explore the role of early division proteins of *Agrobacterium tumefaciens* including 3 FtsZ homologs, FtsA, and FtsW in the transition from polar growth to mid-cell growth and ultimately cell division. Although two of the three FtsZ homologs localize to mid-cell, exhibit GTPase activity and form co-polymers, only one, $FtsZ_{AT}$, is required for cell division. We find that $FtsZ_{AT}$ is required not only for constriction and cell separation, but also for initiation of peptidoglycan synthesis at mid-cell and cessation of polar peptidoglycan biosynthesis. Depletion of $FtsZ_{AT}$ in *A. tumefaciens* causes a striking phenotype: cells are extensively branched and accumulate growth active poles through tip splitting events. When cell division is blocked at a later stage by depletion of FtsA or FtsW, polar growth is terminated and ectopic growth poles emerge from mid-cell. Overall, this work suggests that *A. tumefaciens* FtsZ makes distinct contributions to the regulation of polar growth and cell division.

Graphical Abstract

[#]Address correspondence to Pamela J.B. Brown, brownpb@missouri.edu.
[*]Present address Department of Biochemistry, Stanford University School of Medicine, Stanford, CA 94305

Author contributions

All authors contributed to experimental design, data acquisition, data analysis, and data interpretation. MH, EDG, and PJJB contributed to the writing of the manuscript.

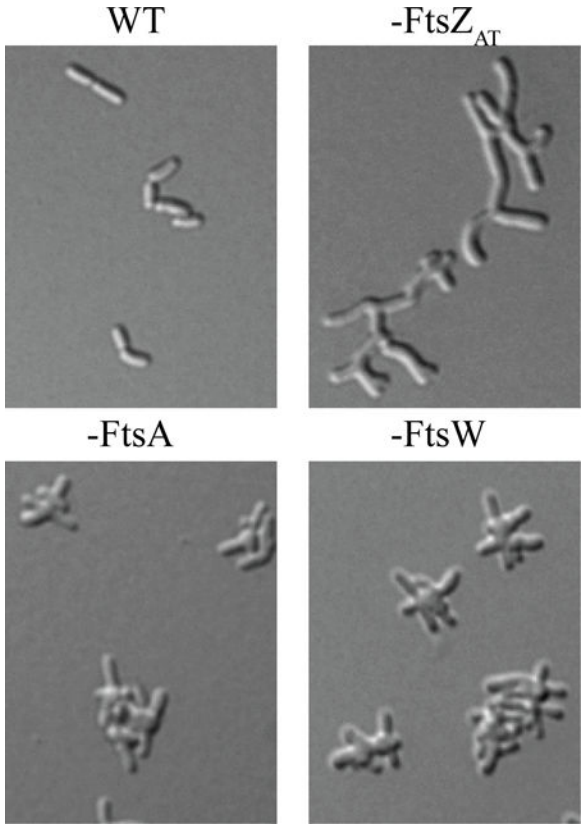

In *Agrobacterium tumefaciens* unipolar elongation is followed by growth at mid-cell, enabling cell division. Remarkably, the absence of $FtsZ_{AT}$ causes growth poles to accumulate due to tip splitting events because peptidoglycan synthesis is not redirected from the growth pole to mid-cell. In contrast, the absence of downstream division proteins, FtsA or FtsW, causes ectopic growth poles to emerge from mid-cell, indicating that these proteins are not necessary for the redirection of growth to mid-cell.

Keywords

Agrobacterium; polar elongation; FtsZ; bacterial cell division; peptidoglycan

Introduction

The spatial and temporal regulation of cell division is a vital process across bacterial species with implications in the development of antimicrobial therapies (den Blaauwen *et al.*, 2014). The cell division process must coordinate membrane invagination(s), peptidoglycan (PG) biosynthesis and remodeling, and the physical separation of the two daughter cells, all while maintaining cellular integrity. Furthermore, cell division must be precisely regulated to be orchestrated with other key cell cycle processes including cell elongation, DNA replication, and chromosome segregation to ensure that each daughter cell is of sufficient size and contains a complete genome (Haeusser & Levin, 2008, Wu & Errington, 2004).

To initiate bacterial cell division, the tubulin-like GTPase, FtsZ, polymerizes and forms a discontinuous ring-like structure at the future site of cell division (Bi & Lutkenhaus, 1991, de Boer *et al.*, 1992, Li *et al.*, 2007, Fu *et al.*, 2010, Holden *et al.*, 2014, Bisson-Filho *et al.*, 2017, Yang *et al.*, 2017). The presence of FtsZ at mid-cell leads to the recruitment of many proteins that function in cell division, collectively called the divisome (Du & Lutkenhaus, 2017, Meier & Goley, 2014, Goley *et al.*, 2011, Erickson *et al.*, 2010). The divisome includes enzymes required for septal PG biosynthesis, such as penicillin-binding protein 3 (PBP3) and FtsW (Du & Lutkenhaus, 2017). Once the divisome is fully assembled, FtsZ filaments treadmill along the circumference of the mid-cell, driving the Z-ring constriction (Yang *et al.*, 2017, Bisson-Filho *et al.*, 2017). The movement of FtsZ filaments is correlated with the movement of enzymes that function in septal PG biogenesis. These finding are consistent with the notion that FtsZ not only recruits enzymes that function in PG biogenesis to mid-cell but also regulates their activities to promote proper cell wall biogenesis (Varma & Young, 2004, Aaron *et al.*, 2007, Sundararajan *et al.*, 2015).

In most rod-shaped model organisms used to study cell division, a block in cell division leads to the production of long, smooth filamentous cells. This phenotype suggests that assembly or activation of some divisome components is necessary not only to enable the cells to divide but also to stop cellular elongation. Indeed, in *Escherichia coli*, FtsZ (along with the Z-ring stabilizing proteins FtsA, ZipA, and ZapA) has been proposed to have an early function in the switch from lateral PG biogenesis to mid-cell PG biosynthesis (Aarsman *et al.*, 2005). Following maturation of the divisome by recruitment of additional PG remodeling enzymes and cell division proteins, PG biosynthesis is coordinated with membrane invagination, enabling cells to constrict and separate (Gray *et al.*, 2015).

Conversely to e.g. *E. coli*, polar growing rods in the alphaproteobacterial clade Rhizobiales exhibit branched morphologies when cell division is blocked (Pini *et al.*, 2015, Howell & Brown, 2016, Pini *et al.*, 2013, Bellefontaine *et al.*, 2002, Cheng *et al.*, 2007, Latch & Margolin, 1997, Fujiwara & Fukui, 1974, Zupan *et al.*, 2013). Examination of the cell morphologies resulting from the block in cell division suggests that different types of branched morphologies arise (Figueroa-Cuilan & Brown, 2018). Drug treatments that block DNA replication cause an early block in cell division, resulting in a “Y” morphology in which the branches are formed from existing growth poles (Latch & Margolin, 1997, Fujiwara & Fukui, 1974). In contrast, antibiotics that target PBP3 cause mid-cell bulges and branches with some cells adopting a “T” or “+” morphologies (Latch & Margolin, 1997, Zupan *et al.*, 2013). These observations suggest that polar-like PG synthesis is redirected to mid-cell when cell division is blocked at a later stage. The manifestation of two distinct phenotypes during early and late blocks in cell division suggests that divisome assembly and activation may contribute to termination of polar growth, onset of mid-cell PG biosynthesis, cell constriction, and ultimately cell separation.

In *Agrobacterium tumefaciens*, homologs of FtsZ and FtsA fused to fluorescent proteins localize at the growth pole during elongation and at mid-cell during division (Brown *et al.*, 2012, Cameron *et al.*, 2014, Zupan *et al.*, 2013). FtsZ was found to arrive at mid-cell considerably earlier than FtsA (Cameron *et al.*, 2014), indicating that FtsZ may be able to initiate Z-ring formation prior to FtsA recruitment to the divisome. This observation is

consistent with the described order of divisome assembly in *Caulobacter crescentus* (Goley *et al.*, 2010) and suggests a distinctive time-dependent role of these proteins in cell division.

Here, we take advantage of the ability to deplete essential proteins in *A. tumefaciens* (Figueroa-Cuilan *et al.*, 2016) to explore the function of cell division proteins FtsZ, FtsA, and FtsW in a polar growing alphaproteobacterium. Although the genome of *A. tumefaciens* encodes three Fts*Z* homologs, we find that only one, henceforth referred to as $FtsZ_{AT}$, is essential for cell survival. $FtsZ_{AT}$ is required to recruit division proteins to mid-cell and likely regulates the activity of PG biosynthesis enzymes at mid-cell. In the absence of $FtsZ_{AT}$, cells not only fail to divide but are also unable to terminate polar growth. Depletion of either FtsA or FtsW also causes a block in cell division, but unlike $FtsZ_{AT}$ depletion, growth at the poles is halted and instead, polar-like PG synthesis is redirected to mid-cell. These observations suggest that only $FtsZ_{AT}$ is required to initiate cell division-specific PG biosynthesis at mid-cell, whereas FtsA and FtsW are exclusively required for cell division. Together these findings suggest that *A. tumefaciens* uses sequential regulation of cell division to ensure that initiation of growth at mid-cell is followed by constriction and ultimately cell separation, a theme that is broadly conserved in bacteria.

Results and Discussion

$FtsZ_{AT}$ is required for cell division and termination of polar growth.

Agrobacterium tumefaciens contains three homologs of *Escherichia coli's* FtsZ, Atu_2086, Atu_4673, and Atu_4215 (Figure 1A) (Zupan *et al.*, 2013). *E. coli* FtsZ comprises three regions: the conserved N-terminal tubulin-like GTPase domain, a C-terminal linker (CTL), and a conserved C-terminal peptide (CTP), which anchors FtsZ to the membrane via interactions with FtsA (Ortiz *et al.*, 2016). Atu_2086 contains each of these domains, out of which the GTPase domain and CTP share 52% and 67% identity to their respective domain in *E. coli* FtsZ, whereas the CTL is extended in length (Zupan *et al.*, 2013). The gene encoding Atu_2086 is found in a putative operon with genes encoding DdlB, FtsQ, FtsA (Wood *et al.*, 2001, Goodner *et al.*, 2001) and is predicted to be essential for cell survival based on a saturating transposon mutagenesis screen (Curtis & Brun, 2014). Atu_2086 localizes to mid-cell in wildtype (WT) pre-divisional cells (Figure 1B) (Brown *et al.*, 2012, Zupan *et al.*, 2013); consistent with a role in cell division. Atu_4673 (called $FtsZ_1$; consistent with the genome annotation) contains a complete GTPase domain with 49% identity to tubulin domain of *E. coli* FtsZ but lacks both the CTL and CTP (Zupan *et al.*, 2013). Although Atu_4673 is not predicted to be required for cell survival based on saturating transposon mutagenesis (Curtis & Brun, 2014), it localizes to mid-cell in pre-divisional cells, suggesting a possible role in cell division (Figure 1B). Atu_4215 (termed $FtsZ_3$ in this work) contains a partial GTPase domain with 48% identity to the N-terminal portion of the *E. coli* FtsZ tubulin domain and lacks both the CTL and CTP (Zupan *et al.*, 2013). $FtsZ_3$ is not essential for survival of *A. tumefaciens* based on saturating transposon mutagenesis (Curtis & Brun, 2014) and exhibits a diffuse localization pattern (Figure 1B). Together, these data suggest that Atu_2086 is the canonical FtsZ protein required for cell division, and this protein will be referred to as $FtsZ_{AT}$ throughout this work (although it is

annotated as $FtsZ_2$ in the *A. tumefaciens* C58 genome (Goodner *et al.*, 2001, Wood *et al.*, 2001)).

To characterize the function of each FtsZ homolog, we constructed deletions of *ftsZ*$_1$ and *ftsZ*$_3$ and a depletion strain of *ftsZ*$_{AT}$. Since we were unable to construct a deletion of *ftsZ*$_{AT}$, we used a depletion strategy in which *ftsZ*$_{AT}$ is present as a single copy under the control of an isopropyl β-D-1-thiogalactopyranoside (IPTG) inducible promoter at a neutral site in the chromosome (Figueroa-Cuilan *et al.*, 2016, Howell & Brown, 2016). Using western blot analysis, we have confirmed the depletion of $FtsZ_{AT}$ in the absence of IPTG (Supplemental Figure 1A).

Deletion of *ftsZ*$_1$ or *ftsZ*$_3$ does not impact cell viability (Figure 1C), cell morphology (Figure 1D; Tables 1; Supplemental Figure 1B), microcolony formation (Figure 1D), constriction rate or position (Table 1) when compared to WT cells. Similarly, when $FtsZ_{AT}$ is expressed via IPTG induction in the depletion strain (labeled in figures as $+FtsZ_{AT}$) the cells remain viable (Figure 1C), are similar in size to WT cells (Table 1), properly position constrictions (Table 1), and form microcolonies (Figure 1D). In contrast, depletion of $FtsZ_{AT}$ (labeled in figures as $–FtsZ_{AT}$) causes a marked decrease in cell viability (Figure 1C) and triggers the formation of large cells with complex branched morphologies (Table 1; Figure 1D). To quantify changes in morphology during depletion of $FtsZ_{AT}$, the cell area of at least 100 cells was calculated based on phase contrast images of cells acquired immediately after removal of the inducer ($-FtsZ_{AT}$ 0 h), 8 h after removal of the inducer ($-FtsZ_{AT}$ 8 h), and 14 h after removal of the inducer ($-FtsZ_{AT}$ 14 h) (Table 1, Supplemental Figure 1C). Initially, the $FtsZ_{AT}$ depleted cells are similar to WT in cell size, but after 8 h of $FtsZ_{AT}$ depletion the cell area has nearly doubled (Table 1, Supplemental Figure 1C). Within 14 h of $FtsZ_{AT}$ depletion, the average cell area has dramatically increased (Table 1, Supplemental Figure 1C). Together, these results demonstrate that only the $FtsZ_{AT}$ homolog is required for proper cell growth and division. The phenotype of cells during $FtsZ_{AT}$ depletion (Movie 1) suggests that $FtsZ_{AT}$ is also required, either directly or indirectly, for the proper termination of polar growth. If a subset of proteins involved in peptidoglycan biosynthesis or remodeling function during both polar elongation and septum formation, establishment of the $FtsZ_{AT}$ ring could lead to disassembly of the polar elongation complex as the shared components are recruited to mid-cell. In addition, or alternatively, the $FtsZ_{AT}$-dependent establishment of new growth poles at mid-cell may trigger the cessation of growth from the old poles.

Deletion of *ftsZ*$_1$ and *ftsZ*$_3$ does not change the $FtsZ_{AT}$ depletion phenotype.

Since the *ftsZ*$_1$ and *ftsZ*$_3$ single deletions do not have an obvious impact on cell morphology, growth, or division, we constructed double and triple mutants to determine if there is an increasing effect when removing multiple *ftsZ* homologs. Double deletion of *ftsZ*$_1$ and *ftsZ*$_3$ does not cause a decrease in cell viability (Figure 2A, top panel), cell morphology (Table 1), or microcolony formation (Figure 2A, bottom panel). Furthermore, *ΔftsZ*$_1$ *ΔftsZ*$_3$ cells properly place constrictions and have an average constriction rate similar to WT (Table 1). Next, we introduced the *ΔftsZ*$_1$, *ΔftsZ*$_3$, and *ΔftsZ*$_1$ *ΔftsZ*$_3$ mutations into the *ftsZ*$_{AT}$ depletion strain to determine if loss of multiple *ftsZ* homologs further aggravated the *ftsZ*$_{AT}$ depletion phenotypes. The combination of the *ftsZ*$_{AT}$ depletion strain with *ΔftsZ*$_1$, *ΔftsZ*$_3$, or

ΔftsZ1 ΔftsZ3 mutations did not result in a further decrease in cell viability (Figure 2B, top panel), worsening of cell morphology (Figure 2B, bottom panel, Table 2), or accumulation of additional growth poles (Table 2) when compared to $FtsZ_{AT}$ depletion alone. Together, these results suggest that the $FtsZ_1$ and $FtsZ_3$ homologs do not have a major impact on cell division under the conditions tested.

ftsZ gene duplications have occurred independently in several alphaproteobacterial lineages and in chloroplasts and some mitochondria (Vaughan *et al.*, 2004). In most of the cases that have been studied, one FtsZ homolog plays a canonical role in cell or organelle division while the other plays a regulatory or specialized role. However, little is known about the roles of multiple FtsZs in certain alphaproteobacteria species. In both *Rhizobium meliloti* and *Magnetospirillum gryphiswaldense*, one of the FtsZs (containing a CTL and CTP similar to $FtsZ_{AT}$) is essential and the other (truncated after the GTPase domain similar to $FtsZ_1$) is dispensable (Margolin & Long, 1994, Muller *et al.*, 2014). In the case of *M. gryphiswaldense*, the truncated *ftsZ* is dispensable for division but important for biomineralization in this magnetotactic species under certain growth conditions. Similarly, it is possible that $FtsZ_1$ or $FtsZ_3$ may have important contributions to cell growth or division of *A. tumefaciens* in different environments such as in its plant-associated life-style.

$FtsZ_1$ requires $FtsZ_{AT}$ to localize to mid-cell and to polymerize *in vitro*.

Since $FtsZ_1$ localizes to mid-cell (Figure 1B), we hypothesized that $FtsZ_1$ may be a nonessential divisome component. To test this, we examined the localization of $FtsZ_1$-sfGFP in both WT and the *ftsZ_AT* depletion strain (Figure 3). In WT and $FtsZ_{AT}$ induced cells, $FtsZ_1$-sfGFP does not localize in newborn cells but forms FtsZ-like rings at the future site of division in pre-divisional cells (Figure 3A, top and middle panel). This Z-like ring constricts to form a single focus in dividing cells. These observations suggest that $FtsZ_1$ may be a divisome component despite the absence of a cell division phenotype in the Δ*ftsZ1* strain. To explore the possibility of interactions arising due to the loss of $FtsZ_1$ and $FtsZ_{AT}$, we next visualized $FtsZ_1$-sfGFP localization during the depletion of $FtsZ_{AT}$ (Figure 3A, bottom panel). We pre-depleted $FtsZ_{AT}$ for 4 h in liquid to avoid cell crowding caused by division events prior to sufficient $FtsZ_{AT}$ depletion. Early during the depletion of $FtsZ_{AT}$, $FtsZ_1$-sfGFP localizes in a FtsZ-like ring near mid-cell. However, as the $FtsZ_{AT}$ depletion continues and branches begin to form, $FtsZ_1$-sfGFP rings and foci progressively fade away, demonstrating that localization of $FtsZ_1$-sfGFP to mid-cell likely requires the presence of $FtsZ_{AT}$.

Since $FtsZ_1$ is likely recruited to mid-cell by $FtsZ_{AT}$, we hypothesized that $FtsZ_{AT}$ and $FtsZ_1$ may form co-polymers. To first test the ability of $FtsZ_{AT}$ and $FtsZ_1$ to independently form polymers, each protein was purified (Supplemental Figure 1D) and subjected to polymerization studies. Right angle light scattering assays of wildtype $FtsZ_{AT}$ revealed that this protein exhibits a GTP-dependent increase in light scattering at concentrations above 2 μm, consistent with its polymerization (Figure 3B, blue lines). Negative stain transmission electron microscopy (TEM) confirmed that $FtsZ_{AT}$ forms gently curved protofilaments in the presence of GTP (Figure 3C, left panel) and it rapidly releases inorganic phosphate suggesting that GTP is hydrolyzed (Figure 3D, blue lines; 4.7 ± 0.2 GTP min^{-1} $FtsZ^{-1}$ at 8

μM $FtsZ_{AT}$, n=3). Surprisingly, we did not observe polymerization of wildtype $FtsZ_1$, even at high protein concentrations either in light scattering (Figure 3B, red line), TEM (Figure 3C, center panel), or GTP hydrolysis assays (Figure 3D, red line).

To determine if $FtsZ_{AT}$ and $FtsZ_1$ can form co-polymers, $FtsZ_1$-L71W and $FtsZ_{AT}$-L72W were purified to enable monitoring of protein polymerization using tryptophan fluorescence (Figure 3E). The leucine to tryptophan mutation introduces a tryptophan on the surface of FtsZ that increases in fluorescence when it is buried in the subunit interface upon polymerization (Chen *et al.*, 2005). While wildtype $FtsZ_{AT}$ (with no tryptophan) does not change in fluorescence on addition of GTP (Figure 3F, solid blue line), $FtsZ_{AT}$-L72W fluorescence increases rapidly after GTP addition reflecting polymerization (Figure 3F, dashed blue line). When wildtype $FtsZ_{AT}$ is added to $FtsZ_{AT}$-L72W, bringing the total FtsZ concentration to 8 μM, fluorescence again increases, but then drops back to baseline upon complete consumption of GTP by this high concentration of FtsZ (Figure 3F, dotted blue line). Conversely, on its own or combined with wildtype $FtsZ_1$, $FtsZ_1$-L71W maintains a constant tryptophan fluorescence level before and after addition of GTP, consistent with our conclusion that it does not polymerize on its own (Figure 3F, red lines). Remarkably, tryptophan fluorescence increases when $FtsZ_1$-L71W and $FtsZ_{AT}$ are mixed, indicating that the $FtsZ_1$-L71W is incorporated into polymers in the presence of $FtsZ_{AT}$ (Figure 3C, purple dashed line). When $FtsZ_{AT}$-L72W is mixed with $FtsZ_1$, fluorescence increases above the level observed for $FtsZ_{AT}$-L72W alone and drops to baseline faster than $FtsZ_{AT}$-L72W on its own, again indicating co-polymerization. Finally, equimolar concentrations of $FtsZ_{AT}$ alone or mixtures of $FtsZ_{AT}$ and $FtsZ_1$ exhibit similar rates of GTP hydrolysis (Figure 3D) and form qualitatively similar polymers by TEM (Figure 3C, right panel). Together, these observations indicate that $FtsZ_1$ cannot polymerize independently, but that $FtsZ_{AT}$ and $FtsZ_1$ form co-polymers with similar structure and GTP hydrolysis rates as $FtsZ_{AT}$ polymers.

Though multiple FtsZs are present in a number of bacterial and chloroplast lineages, their co-assembly properties have only begun to be characterized. In contrast to our observations, each copy of FtsZ in *M. gryphiswaldense* was able to independently polymerize *in vitro*, but they also appeared to directly interact, perhaps reflecting an ability to co-polymerize (Muller *et al.*, 2014). Chloroplast FtsZs from *Arabadopsis thaliana* are also able to co-polymerize and, at least under some conditions, to independently polymerize (Olson *et al.*, 2010). Conversely, one of the FtsZs from tobacco chloroplasts cannot polymerize on its own but promotes polymerization of its partner homolog (El-Kafafi el *et al.*, 2005). Finally, the FtsZ pair from the chloroplasts of representative green and red algae co-polymerize into polymers with altered assembly dynamics from either homopolymer (TerBush *et al.*, 2018). It is likely that in each of these cases, the assembly or co-assembly properties of the duplicated FtsZs have evolved to suit a niche regulatory function. We hypothesize the $FtsZ_1$ from *A. tumefaciens* has low affinity for itself, but higher affinity for $FtsZ_{AT}$, limiting its homopolymerization but allowing for co-polymerization both *in vitro* and in cells. Since $FtsZ_1$ cannot polymerize independently, $FtsZ_{AT}$ must first polymerize at mid-cell after which $FtsZ_1$ can be recruited by co-polymerization. The biological relevance of these biochemical and cell biological properties awaits further study.

$FtsZ_{AT}$ depletion results in tip splitting events.

Once we identified $FtsZ_{AT}$ as the primary homolog involved in cell division we next analyzed the growth phenotype during $FtsZ_{AT}$ depletion more carefully. Compared to $FtsZ_{AT}$ induced cells (Figure 4A, top), observation of cells during $FtsZ_{AT}$ depletion by time-lapse microscope reveals remarkable changes in cell morphology (Figure 4A, bottom; Movie 1). Early during the depletion of $FtsZ_{AT}$, an ectopic pole forms near mid-cell. We hypothesize that this occurs due to the ability of the remaining $FtsZ_{AT}$ to identify the mid-cell and recruit PG biosynthesis machinery to that site. Both the original growth pole and the ectopic pole are growth-active, resulting in the presence of multiple growth poles. These growth poles are unable to terminate cell elongation and ultimately most growth active poles are split, leading to the accumulation of many growth active poles (Figure 4A, bottom; Movie 1; Table 2) and the rapid increase in cell area (Table 1; Supplemental Figure 1C) until the cell lyses.

The branched morphology observed during $FtsZ_{AT}$ depletion is in stark contrast to FtsZ depletion observed in other organisms. In species like *E. coli* and *B. subtilis*, which utilize laterally localized peptidoglycan biosynthesis during elongation, depletion of FtsZ results in long, smooth filamentous cells. We hypothesize that the branching morphology of the *A. tumefaciens* $FtsZ_{AT}$ depletion strain can be attributed to polar elongation. During the block in cell division, the growth pole continues to grow and presumably recruits additional peptidoglycan biosynthesis proteins. This could lead to an over-accumulation of proteins involved in cellular elongation causing the pole to split into two poles. A similar branching pattern has been characterized during typical growth of *Streptomyces coelicolor* (Richards *et al.*, 2012). In this polar growing bacterium, the established complex of proteins contributing to elongation splits, leaving a small portion of the protein complex behind as growth continues. With time, the subpolar complex of proteins accumulates in size and eventually establishes a new growth pole. Although the polar growth molecular mechanisms are not conserved between *A. tumefaciens* and *S. coelicolor*, the fundamental principle of tip splitting as a consequence of polar growth appears to be shared.

PopZ-YFP accumulates at growth poles in the absence of $FtsZ_{AT}$.

In WT *A. tumefaciens*, deletion of *popZ* has been shown to cause ectopic poles and cells devoid of DNA, demonstrating a role in coordinating cell division with chromosome segregation (Howell *et al.*, 2017a, Ehrle *et al.*, 2017). We hypothesize that PopZ-dependent coordination of cell division likely involves FtsZ. In WT, PopZ-YFP localizes to the growing pole during elongation and is recruited to mid-cell just prior to cell separation (Figure 4B, top panel) (Ehrle *et al.*, 2017, Howell *et al.*, 2017a, Grangeon *et al.*, 2015). In some freshly divided cells PopZ-YFP can be visualized at both the growing pole as well as the old pole resulting in an average of 1.12 PopZ-YFP labeled poles per cell (100 cells analyzed SD +/− . 33). When $FtsZ_{AT}$ is expressed in the *ftsZ*$_{AT}$ depletion strain, PopZ-YFP has a similar localization pattern as in WT cells (Figure 4B, middle panel). When $FtsZ_{AT}$ is depleted, PopZ-YFP stays at the growth poles and as tip splitting events lead to the production of new growth poles, PopZ-YFP appears to be split and retained at all growth active poles (Figure 4B, bottom panel). The accumulation of growing poles results in a population with an average 7.11 poles per cell containing PopZ-YFP (100 cells analyzed after 14 hours of $FtsZ_{AT}$ depletion, SD +/− 2.65). These observations indicate that $FtsZ_{AT}$ is required for

recruitment of PopZ from the growth pole to mid-cell. Remarkably, both $FtsZ_{AT}$ and FtsA are mislocalized in the absence of PopZ, leading to the establishment of asymmetric constriction sites and a broad range of cell lengths (Howell *et al.*, 2017a). Together, these data suggest that the presence of both PopZ and FtsZ are important for proper positioning and functioning of the divisome.

Loss of septal PG synthesis results in altered total PG composition.

Since polar growth appears to continue in the absence of $FtsZ_{AT}$ (Figure 4A, bottom panel), we used fluorescent-D-amino acids (FDAAs), to probe sites enriched in peptidoglycan synthesis (Kuru *et al.*, 2012) during depletion of $FtsZ_{AT}$. In WT cells and conditions in which $FtsZ_{AT}$ is expressed in the depletion strain, FDAAs localize at a single pole in elongating cells and at mid-cell in pre-divisional cells (Figure 4C, top) (Kuru *et al.*, 2012). As $FtsZ_{AT}$ is depleted, FDAAs are targeted strictly to the poles, confirming that polar peptidoglycan synthesis is responsible for the observed increase in cell biomass after 8 h and 14 h of depletion (Figure 4C, bottom).

Since cells depleted of $FtsZ_{AT}$ fail to terminate polar growth and do not produce septal peptidoglycan, we hypothesized that the peptidoglycan composition may reveal chemical signatures of peptidoglycan derived from polar growth. Thus, we characterized the peptidoglycan composition of both WT cells and the *ftsZ*$_{AT}$ depletion strain in both the presence and absence of IPTG using ultra-performance liquid chromatography (UPLC) (Alvarez *et al.*, 2016). The major muropeptides found in WT *A. tumefaciens* PG and their quantification are shown in (Supplemental Figure 2A) and include monomeric (M), dimeric (D), and trimeric (T) muropeptides. The muropeptide composition and abundance is similar between WT cells, WT cells grown in the presence of IPTG, and the *ftsZ*$_{AT}$ depletion strain grown in the presence of IPTG such that $FtsZ_{AT}$ is expressed (Supplemental Figure 2B). These findings suggest that there are no major changes in PG composition due to IPTG and that the presence of IPTG leads to complementation in the *ftsZ*$_{AT}$ depletion strain. In contrast, when the *ftsZ*$_{AT}$ depletion strain is grown in the absence of IPTG for 14 h, marked changes in muropeptide composition are observed (Figure 4D, Supplemental Figure 2C-D). When $FtsZ_{AT}$ is depleted, there is a significant increase in LD-crosslinkage as well as a decrease in total DD-crosslinkage (Figure 4D). These data suggest that the activity of LD-transpeptidases is increased and the activity of PBP-mediated DD-transpeptidases is decreased during $FtsZ_{AT}$ depletion.

The *A. tumefaciens* genome contains 14 LD-transpeptidases, 7 of which are specific to Rhizobiales. The Rhizobiales-specific LD-transpeptidase encoded by *Atu_0845* (referred to here as $LDTP_{0845}$) has been shown to localize to the growing pole in WT cells and has been hypothesized to contribute to polar growth (Cameron *et al.*, 2014). This localization pattern was confirmed in both WT and $FtsZ_{AT}$ induced cells (Figure 4E). $LDTP_{0845}$ is frequently found only at the growth pole, but also can exhibit a bipolar localization pattern. Quantification reveals that $LDTP_{0845}$ localizes to an average of 1.18 poles per WT cell and 1.17 poles per cell expressing $FtsZ_{AT}$ in the depletion strain (100 cells analyzed for each strain). We find that $LDTP_{0845}$ localizes at 7.09 growth poles per cell following 14 hours of $FtsZ_{AT}$ depletion (100 cells analyzed) (Figure 4E, bottom). This observation suggests that

this $LDTP_{0845}$ may contribute to changes in PG composition during $FtsZ_{AT}$ depletion and supports a potential role for LD-transpeptidases in polar growth during elongation. Since there are 14 LDTPs in *A. tumefaciens* and thus far our preliminary data suggests that deleting any one of them does not cause a defect in polar growth, we suspect that redundant LDTPs likely contribute to polar growth.

FtsA is required for cell division but not initiation of growth from mid-cell.

FtsA is an actin-like protein that associates with the membrane through an amphipathic helix and binds the FtsZ CTP to anchor FtsZ polymers to the membrane (Pichoff & Lutkenhaus, 2007, Szwedziak *et al.*, 2012). In *C. crescentus*, recruitment of FtsA to mid-cell occurs well after the establishment of the FtsZ-ring and is dependent on the presence of FtsZ (Moll & Thanbichler, 2009, Goley *et al.*, 2011). In *A. tumefaciens*, FtsA-sfGFP is retained at the growth pole prior to appearing at mid-cell just before cell division (Zupan *et al.*, 2013, Cameron *et al.*, 2014). Here, we confirm that FtsA-sfGFP is observed as a focus at the growth pole until transitioning to a ring-like structure at mid-cell (Figure 5A, top panel) At some timepoints, both a polar focus and a mid-cell ring of FtsA are observed (Figure 5A, top panel, 130 min). Eventually, the polar focus disappears as the FtsA-sfGFP ring becomes more intense just prior to cell division. During the depletion of $FtsZ_{AT}$, a focus of FtsA-sfGFP can be found at the growing pole, and at a newly formed ectopic pole near mid-cell (Figure 5A, bottom panel). FtsA-sfGFP remains associated with each growth pole, and as the poles undergo tip splitting events, each focus of FtsA-sfGFP is also split, resulting in the presence of FtsA-sfGFP in each of the 4 growth-active poles. These observations suggest that $FtsZ_{AT}$ is required for proper localization of FtsA to mid-cell prior to cell division.

Since FtsA tethers FtsZ to the membrane and enables divisome assembly (Vaughan *et al.*, 2004, Szwedziak *et al.*, 2012, Ma & Margolin, 1999) in *E. coli*, we expected that the depletion of FtsA would phenocopy the depletion of FtsZ. Although a saturating transposon mutagenesis screen indicated that *ftsA* is not essential for *A. tumefaciens* cell survival (Curtis & Brun, 2014), we were unable to construct a Δ*ftsA* mutant. Thus, we constructed a depletion strain in which expression of *ftsA* is controlled by P_{lac}. Under conditions where FtsA is present in the *ftsA* depletion strain, cells maintain proper rod-shaped morphology, polar growth, and cell division occurs from constrictions formed near mid-cell (Figure 5B-C, top panels). In contrast, when FtsA is depleted, cells exhibit a marked change in morphology (Figure 5B, bottom panel; Movie 2). During the depletion of FtsA, rod-shaped cells initially elongate from a growth pole (Figure 5B, bottom panel, 0 min). Polar growth is terminated and growth is re-initiated from near mid-cell, typically resulting in the formation of two ectopic poles perpendicular to the original longitudinal axis of the cell (Figure 5B, bottom panel, 170 min). Cells depleted of FtsA continue multipolar growth (Figure 5B, bottom panel, 360 min), terminate growth from both poles and reinitiate growth from near mid-cell resulting in the formation of a new pair of ectopic growth poles (Figure 5B, bottom panel, 510 min). This pattern of multipolar growth, polar growth termination, and new branch formation is continued until cells eventually bulge at the mid-cell and lyse. Overall these observations indicate that the phenotypes caused by $FtsZ_{AT}$ and FtsA depletion are distinct from one another and suggest that only FtsZ is required for initiation of PG biosynthesis at mid-cell and the cessation of polar growth.

To confirm that polar growth occurs and is terminated during FtsA depletion, cells were labeled with FDAAs (Figure 5C, bottom panel). Indeed, FDAAs label the tips of two poles, which are emerging from near mid-cell consistent with the re-initiation of polar growth. To further confirm that polar growth is terminated during FtsA depletion, we observed the localization of PopZ-YFP as FtsA is depleted (Figure 5D, top panel). PopZ marks the growth poles (Grangeon *et al.*, 2015) and becomes trapped at growth poles during depletion of FtsZ (Figure 4B). During FtsA depletion, PopZ-YFP is initially present at the growth pole (Figure 5D, top panel, 0 min). Next, PopZ-YFP disappears from the growth poles and reappears near mid-cell (Figure 5D, top panel, 80 min) indicating that growth is redirected to mid-cell. Throughout the FtsA depletion, PopZ-YFP continues to disappear from growth poles and reappears at the tips of newly emerging growth poles. Overall, these observations clearly indicate that FtsA is not necessary for termination of polar growth and initiation of growth from mid-cell; however, FtsA has an essential function at a later stage of cell division since the cells fail to divide and are prone to lysis.

The ability of cells to target growth to near mid-cell during FtsA depletion suggests that FtsZ-rings may form, enabling the termination of polar growth. Indeed, $FtsZ_{AT}$-sfGFP-rings form near mid-cell early during FtsA depletion (Figure 5D, bottom panel). $FtsZ_{AT}$-sfGFP is briefly retained at new growth poles before reappearing to mark the site where a new growth pole will emerge. These observations are consistent with the finding the FtsA is retained at the growth pole longer than FtsZ (Cameron *et al.*, 2015, Zupan *et al.*, 2013), and suggest that FtsA arrives at mid-cell after Z-ring assembly and the initiation of FtsZ-dependent cell wall biogenesis. The results observed here in *A. tumefaciens* are consistent with the observation that FtsA arrives to mid-cell after FtsZ and the onset of mid-cell cell wall biogenesis in *C. crescentus* (Moll & Thanbichler, 2009, Goley *et al.*, 2011). In both *A. tumefaciens* and *C. crescentus*, the late arrival of FtsA to the divisome suggests that other proteins contribute to proper tethering of FtsZ to the membrane. In *C. crescentus*, the FtsZ-binding protein, FzlC, functions as a membrane anchor early during the establishment of the divisome (Goley *et al.*, 2010, Meier *et al.*, 2016). A homolog of FzlC is readily found in the *A. tumefaciens* genome (Atu2824) and may contribute to the ability of FtsZ-rings to form in the absence of FtsA.

Depletion of the downstream divisome component FtsW phenocopies depletion of FtsA.

Having observed a distinct effect on cell morphology in the absence of *ftsA*, we wondered if the phenotype observed during *ftsA* depletion could be recapitulated in the absence of another late-arriving divisome protein. To test this hypothesis, we constructed a depletion strain of FtsW, which is recruited to mid-cell after FtsA in both *E. coli* and *C. crescentus* divisome assembly models (Goley *et al.*, 2011, Du & Lutkenhaus, 2017). Depletion of FtsW results in a phenotype which is strikingly similar to the depletion of FtsA (Figure 6). When FtsW is induced normal growth is observed (Figure 6A, top panel). During FtsW depletion, polar growth is terminated, resulting in the establishment of growth-active poles from near mid-cell (Figure 6A, bottom panel; Movie 3). Multiple rounds of termination of polar growth followed by reinitiation of growth from near mid-cell occur until the mid-cell bulges and the cells ultimately lyse (Figure 6A, bottom panel). Labeling of growth active poles with FDAAs (Figure 6B) or by tracking PopZ-YFP localization (Figure 6C, top panel) confirmed that new branches which emerge from mid-cell are formed by polar growth. Finally, we

confirmed that FtsZ-rings form during the depletion of FtsW and the presence of an $FtsZ_{AT}$-sfGFP-ring typically marks the site where an ectopic growth pole will form (Figure 6C, bottom panel). Together, these observations suggest that FtsZ-rings are formed in the absence of FtsW, enabling the initiation of cell wall biogenesis. Given that FtsW likely drives septal PG biosynthesis, (Fraipont *et al.*, 2011) these findings indicate that the cell wall biogenesis that occurs during depletion of FtsA or FtsW may require the elongation machinery, which typically functions in polar growth. Since the elongation machinery for *A. tumefaciens* remains to be identified, it is possible that there is considerable overlap between the machineries that contribute to polar and septal PG biosynthesis.

Concluding Remarks

While many questions remain unanswered about the regulation of cell wall biogenesis in *A. tumefaciens*, our work sheds light on the transition from polar growth to mid-cell growth. We find that $FtsZ_{AT}$, FtsA, and FtsW are required for constriction and cell separation, but $FtsZ_{AT}$ is also required to terminate polar growth and initiate mid-cell peptidoglycan synthesis. How might the formation of an $FtsZ_{AT}$-ring at mid-cell cause the termination of polar growth? We find that PopZ, and $LDTP_{0845}$ become trapped at the growth poles during FtsZ depletion (Figure 5). It is possible that one or more of these proteins contributes to both polar peptidoglycan biosynthesis and mid-cell peptidoglycan synthesis and that the FtsZ-dependent targeting of these proteins (and likely others) to mid-cell triggers the termination of polar growth. While the mid-cell localization of PopZ is dependent on the presence of $FtsZ_{AT}$ (Figure 4), $FtsZ_{AT}$-ring stability and placement are impacted by the absence of PopZ (Howell *et al.*, 2017a). Furthermore, deletion of *popZ* impairs termination of polar growth and results in cell division defects (Howell *et al.*, 2017a, Ehrle *et al.*, 2017, Grangeon *et al.*, 2017). The apparent co-dependence of FtsZ and PopZ for localization may suggest that these proteins function together during the early stages of cell division, particularly the termination of polar growth and onset of mid-cell PG biosynthesis.

Overall, our results are consistent with a general model, which is highly conserved in bacteria, in which the establishment of a FtsZ-ring leads to the recruitment of many other cell division proteins to mid-cell (Du & Lutkenhaus, 2017), though many mechanistic questions remain. How is $FtsZ_{AT}$ targeted to mid-cell? A variety of mechanisms that contribute to the proper placement of FtsZ at mid-cell have been described (for review see (Rowlett & Margolin, 2015, Monahan *et al.*, 2014)). The most well studied mechanisms of FtsZ positioning include negative regulation by the Min system and nucleoid occlusion. While genes encoding components of the Min system are readily identifiable in the *A. tumefaciens* genome, the deletion of *minCDE* has a minimal impact on placement of constriction sites and cell division efficiency (Flores *et al.*, 2018). Furthermore, $FtsZ_{AT}$-GFP rings form over DNA prior to nucleoid separation in *A. tumefaciens*. These observations indicate that additional regulatory mechanisms must contribute to proper division site selection in *A. tumefaciens*. Following the appearance of FtsZ at mid-cell, how is the $FtsZ_{AT}$-ring stabilized? In *E. coli*, the FtsZ-ring is stabilized by interactions with FtsA and ZipA, which tether FtsZ filaments to the membrane (Ma & Margolin, 1999, Mosyak *et al.*, 2000, Haney *et al.*, 2001, Szwedziak *et al.*, 2012). In *A. tumefaciens*, $FtsZ_{AT}$ appears at mid-cell well before FtsA (Cameron *et al.*, 2014) and we observe that $FtsZ_{AT}$ rings form even

when FtsA is depleted (Figure 5D, bottom panel). Furthermore, the position of $FtsZ_{AT}$-GFP rings marks the site of ectopic pole formation. These observations suggest the $FtsZ_{AT}$ is stabilized, at least early during cell division by other proteins. While there are no obvious ZipA homologs encoded in the *A. tumefaciens* genome, a homolog of FzlC, which functions to stabilize FtsZ in *C. crescentus* (Goley *et al.*, 2010, Meier *et al.*, 2016), is encoded in the genome.

The observation that FtsZ is necessary for the initiation of mid-cell PG biosynthesis suggests that FtsZ is necessary for recruitment of PG biosynthesis enzymes to mid-cell. Septal PG biosynthesis is likely mediated by FtsW, a putative PG glycosyltransferase (Cho *et al.*, 2016, Meeske *et al.*, 2016, Emami *et al.*, 2017), and PBP3 (FtsI), a PG DD-transpeptidase (Botta & Park, 1981). In *A. tumefaciens*, depletion of FtsW does not cause a complete block of PG synthesis at mid-cell (Figure 5). This observation suggests that mid-cell PG biosynthesis is mediated by other cell wall biogenesis enzymes while the activity of FtsW contributes to later stages of cell division, consistent with the inability of cells to form constrictions and separate in the absence of FtsW. These observations may indicate that the initial PG biosynthesis at mid-cell comprises the final stage of cell elongation, consistent with descriptions of FtsZ-dependent mid-cell elongation in *C. crescentus* (Aaron *et al.*, 2007). The observation that growth-active, ectopic poles emerge from near mid-cell during FtsW depletion (Figure 5B) provides evidence in support of this possibility. Thus, FtsZ-dependent PG biosynthesis may contribute to both elongation and cell division in *A. tumefaciens*. For a polar growing bacterium, it is tempting to speculate that the retention of PG biosynthesis machinery dedicated to elongation at the site of cell division may prime the newly formed poles to become growth active following cell separation.

Experimental Procedures

Bacterial strains and culture conditions.

All bacterial strains and plasmids used are listed in Table S1. *A. tumefaciens* strains were grown in ATGN minimal medium with .5% glucose (Morton & Fuqua, 2012a) at 28°C. *E. coli* strains were grown in Luria-Bertani medium at 37°C. When indicated, kanamycin (KM) was used at 300 μg ml^{-1} for *A. tumefaciens*, 50 μg ml^{-1} for *E. coli* DH5α, and 25 μg ml^{-1} for *E. coli* S17–1 λ *pir*. Gentamicin was used when indicated at 200 μg ml^{-1} for *A. tumefaciens* and 20 μg ml^{-1} for *E. coli* DH5α. IPTG was added at a concentration of 1 mM when indicated. Cumate was added at a concentration of 0.1 mM when indicated.

Construction of expression plasmids and strains.

All strains and plasmids used are listed in Table S1, while primers used are listed in Table S2. For amplification of target genes, primer names indicate the primer orientation and added restriction sites. To construct expression vectors containing *$ftsZ_{AT}$-sfgfp*, *$ftsZ_1$-sfgfp*, *$ftsZ_3$-sfgfp*, and *$ldtp_{0845}$-sfgfp* the respective coding sequence was amplified from purified C58 genomic DNA using primers indicated in Table S4.2. The amplicons were digested overnight and ligated into cut pSRKKM-P_{lac}-*sfgfp* using NEB T4 DNA ligase at 4°C overnight. The newly formed *sfgfp* fusion of each gene was excised from the plasmid by overnight digestion with NdeI and NheI. Fragments containing *$ftsZ_{AT}$-sfgfp*, *$ftsZ_1$-sfgfp*,

ftsZ$_3$-*sfgfp*, and *ldtp*$_{0845}$-*sfgfp* were then ligated into cut pRV-MCS2 to give constitutive expression vectors containing the fusions. To construct the *popZ-yfp* expression vector, *popZ* along with the upstream promoter sequence were amplified from purified C58 genomic DNA, digested and ligated into pMR10 containing YFP.

Construction of deletion/depletion plasmids and strains.

Vectors for gene deletion by allelic exchange were constructed using recommended methods for *A. tumefaciens* (Morton & Fuqua, 2012b). Briefly, 500 bp fragments upstream and downstream of the target gene were amplified using primer pairs P1/P2 and P3/P4 respectively. Amplicons were spliced by overhang extension (SOE) using primer pair P1/P4. The amplicon was digested and ligated into pNTPS139. The deletion plasmids were introduced into *A. tumefaciens* by mating using an *E. coli* S17 conjugation strain to create kanamycin (KM) resistant, sucrose sensitive primary exconjugants. Primary exconjugants were grown overnight in media with no selection. Secondary recombinants were screened by patching for sucrose resistance and KM sensitivity. Colony PCR with primers P5/P6 for the respective gene target was used to confirm deletion. PCR products from P5/P6 primer sets were sequenced to further confirm deletions.

For depletion strains, target genes (*ftsZ*$_{AT}$, *ftsA*, and *ftsW*) were amplified, digested and ligated into either pUC18-mini-Tn*7*T-GM-P$_{lac}$ or pUC18-mini-Tn*7*T-GM-P$_{lac}$. The mini-Tn*7* vectors, along with the pTNS3 helper plasmid, were introduced into C58Δ*tetRA*::a-*att*Tn*7* as described previously (Figueroa-Cuilan *et al.*, 2016). Transformants were selected for gentamicin resistance and insertion of the target gene into the a-*att* site was verified by colony PCR using the tet forward and Tn7R109 primer. PCR products were sequenced to confirm insertion of the correct gene. Next, the target gene was deleted from the native locus as described above in the presence of 1 mM IPTG to drive expression of the target gene from the engineered site.

Construction of plasmids for protein expression and purification.

To construct pET21a FtsZ$_{AT}$, *ftsZ*$_{AT}$ was amplified from C58 genomic DNA with FtsZ$_{AT}$ For NdeI and FtsZ$_{AT}$ Rev EcoRI, digested with NdeI and EcoRI, and ligated into similarly digested pET21a. To construct pTB146 FtsZ$_1$, *ftsZ*$_1$ was amplified from C58 genomic DNA with FtsZ$_1$ For SapI and FtsZ$_1$ Rev BamHI, digested with SapI and BamHI, and ligated into similarly digested pTB146. Ligation products were transformed into NEB Turbo (New England Biolabs) and selected for ampicillin resistance. Insertions were verified by colony PCR and Sanger sequencing. Primers FtsZ$_{AT}$-L72W and FtsZ1-L71W were used to mutagenize pET21a FtsZ$_{AT}$ and pTB146 FtsZ$_1$, respectively, using the Quikchange Multi Lightning Mutagenesis Kit (Agilent) and following the manufacturer's protocol to generate pET21a FtsZ$_{AT}$-L72W and pTB146 FtsZ$_1$-L71W. Mutations in the targeted sites were verified by Sanger sequencing.

DIC and phase contrast microscopy.

Exponentially growing cells (OD$_{600}$ = ~0.6) were spotted on 1% agarose ATGN pads as previously described (Howell *et al.*, 2017b). Microscopy was performed with an inverted Nikon Eclipse TiE with a QImaging Rolera em-c^2 1K EMCCD camera and Nikon Elements

Imaging Software. For time-lapse microscopy, images were collected every ten minutes, unless otherwise stated.

Fluorescence microscopy.

Plasmid encoded $FtsZ_{AT}$-sfGFP, $FtsZ_1$-sfGFP, $FtsZ_3$-sfGFP, and $LDTP_{0845}$-sfGFP fusions were expressed from the P_{van} promoter, which provides constitutive low levels of expression (Figure 6- Figure Supplement 1C). To construct demographs of various FtsZ-sfGFP localization, at least 225 cells were imaged for each strain. A GFP channel profile was taken along the medial axis for each cell imaged. These medial axis profiles were then aligned by cell length using MicrobeJ software (Ducret *et al.*, 2016).

Plasmid encoded FtsA-sfGFP and PopZ-YFP fusions were expressed from the native promoters. Cells containing plasmids with fluorescent protein fusions were grown to exponential phase before imaging on agarose pads.

To visualize sites of active peptidoglycan synthesis 1 ml of exponentially growing cells was labeled with 5 μl of 5mM fluorescent D-amino acid (FDAA), HCC amino-D-alanine (HADA) for 1 minute and washed three times to remove residual label from the supernatant, as previously described (Kuru *et al.*, 2012, Howell *et al.*, 2017b).

Cell viability and growth curve assays.

For cell viability spot assays, cells were grown with IPTG to exponential phase before washing 3 times to remove inducer. Cells were then diluted to OD_{600} = 0.1 and serially diluted in ATGN (no inducer). 3 μl of each dilution was spotted onto ATGN and incubated at 28°C for 3 days before imaging. When appropriate ATGN plates contained KM 300 μg ml^{-1}, and IPTG 1mM as indicated in figure legends. For growth curve analysis, exponentially growing cultures were diluted to OD_{600} = .05 in 200 μl of ATGN in 96-well plates. Plates were shaken for 1 minute before OD_{600} readings, which were taken every 10 minutes.

Cell morphology and constriction rate analysis.

Exponentially growing cells were imaged using phase contrast microscopy as described above. Cell length, area, and constrictions were detected using MicrobeJ software (Ducret *et al.*, 2016). To calculate constriction rates, cells with detectable constrictions were tracked using time-lapse microscopy. The width of the cell constriction was measured at an initial time-point and the measurement was repeated after 10 minutes. The difference in constriction width was divided by the 10-minute time interval to give a constriction rate.

To quantify the number of growth active and inactive poles, cells were grown to exponential phase with IPTG and washed 3 times before adding fresh media with or without IPTG. Cells were cultured under normal growth conditions for 14 hours before labelling active growth poles with FDAAs as described above. FDAA labelled poles were then quantified using MicrobeJ software.

Western blot analysis.

For western blot analysis of FtsZ depletion, the *ftsZ* depletion strain was grown in 40 ml ATGN with 1 mM IPTG to exponential phase. 2 ml of culture was collected prior to depletion (time 0) by centrifugation at 10,000 x *g* for 3 minutes. The remaining culture was collected by centrifugation at 3500 x *g* for 10 minutes, and supernatants were discarded. Cells were washed in sterile water and pelleted again. To deplete FtsZ, the pellet was resuspended in fresh ATGN without IPTG and grown under standard culturing conditions. 2-ml samples were collected by centrifugation after 30, 45, 60, 120, and 240 minutes of depletion. OD_{600} was taken for each sample prior to centrifugation so that samples could be normalized to an OD_{600} equivalent to 0.68. The cell pellets were incubated with 100 μl of a master mix containing 1 ml of BugBuster protein extraction reagent (Novagen) and supplemented with 1 EDTA-free protease inhibitor cocktail (Sigma), 10 μl of lysonase (Novagen), 2,500 U ml^{-1} DNase I (Thermo Scientific), and 1 mM dithiothreitol (DTT) (Thermo Scientific) for 25 minutes with shaking at room temperature to lyse the cell pellets. The whole-cell lysates were clarified by centrifugation at 10,000 rpm for 15 min. A final concentration of 1 X Laemmli buffer was added to the cleared cell lysates. Samples were boiled at 100°C for 5 min prior to loading on a 4–15% Mini-PROTEAN TGX Precast Gel (Bio-Rad). The separated proteins were electroblotted onto polyvinylidene difluoride (PVDF) membranes (Bio-Rad) and blocked overnight in 5% nonfat dry milk powder solubilized in 1% TBST (Tris-buffered saline [TBS], 1% Tween 20). The blocked PVDF membranes were probed with *Escherichia coli* anti-FtsZ serum at a final concentration of 1/3000 ((Ward & Lutkenhaus, 1985), gift from Joe Lutkenhaus) for 1.5 h in 5% milk-TBST, followed by incubation with anti-rabbit (1:5000) HRP (Pierce 31460) secondary antibody for 1 h in 5% milk-TBST. The secondary antibody was detected using the ECL Plus HRP substrate (Thermo Scientific Pierce).

Protein expression and purification.

$FtsZ_{AT}$ and $FtsZ_{AT}$-L72W were expressed and purified in untagged form. Each was produced from a pET21 expression vector (pEG1555 – $FtsZ_{AT}$, pEG1556 - $FtsZ_{AT}$-L72W,) in *Escherichia coli* Rosetta(DE3)pLysS induced at 37°C for 4 h with 0.5 mM IPTG after OD reached 0.8 to 1.0 OD at 600 nm. Cells were harvested by centrifugation at 6000 x g and resuspended in 30 mL FtsZ QA buffer (50 mM Tris-HCl pH 8, 50 mM KCl, 0.1 mM EDTA, 10% glycerol) per liter of culture. Resuspensions were snap frozen in liquid nitrogen and stored at −80°C until purification. To purify, resuspensions were thawed quickly and cells were lysed by incubation with 1 mg ml^{-1} lysozyme, 2.5 mM $MgCl_2$, DNAse I, 2 mM PMSF, and a complete mini EDTA-free protease inhibitor tablet (Roche) for 45 min to 1 h at room temperature followed by sonication. Lysates were cleared by centrifugation at 15000 x g for 30 min at 4°C and filtered through a 0.45 μm filter before anion exchange chromatography (HiTrap Q HP 5 mL, GE Life Sciences). Protein was eluted with a linear KCl gradient (FtsZ QA buffer with 50 to 500 mM KCl) and fractions containing FtsZ were verified by SDS-PAGE, pooled, and subjected to ammonium sulfate precipitation. Precipitates (at 17–20% ammonium sulfate saturation depending on the variant) were verified by SDS-PAGE, resuspended in HEK50G (50 mM HEPES-KOH pH 7.2, 0.1 mM EDTA, 50 mM KCL, 10% glycerol, 1 mM β-mercaptoethanol), and further purified by gel filtration (Superdex 200

10/300 GL, GE Life Sciences). Peak fractions were pooled, snap frozen in liquid nitrogen, and stored at −80°C.

$FtsZ_1$ and $FtsZ_1$-L71W were produced as His_6-SUMO fusions and cleaved to yield untagged, scarless proteins. Each was produced from a pTB146 expression vector (pEG1535 - $FtsZ_1$, pEG1542 - $FtsZ_1$-L71W) in *E. coli* Rosetta (DE3)pLysS as described above. Cells were harvested by centrifugation as above, resuspended in HK300G (50 mM HEPES-KOH pH7.2, 300 mM KCl, 10% glycerol) with 20 mM imidazole, snap frozen in liquid nitrogen, and stored at −80°C until purification. To purify, resuspensions were thawed quickly and cells were lysed by incubation with 1 mg ml^{-1} lysozyme, 2.5 mM $MgCl_2$, and DNase I for 45 min at room temperature followed by sonication. Lysate was cleared and filtered as described above. Protein was isolated by Ni^{2+} affinity chromatography (HisTrap FF 1 mL, GE Life Sciences) and eluted in HK300G with 300 mM imidazole. Fractions containing His_6-SUMO fusions were verified by SDS-PAGE, combined with Ulp1 Sumo protease at a 1:100 (protease:FtsZ) molar ratio, and cleaved by incubation at 30°C for 3.5 h. Cleaved $FtsZ_1$ or $FtsZ_1$L71W was purified away from His_6-SUMO by gel filtration (Superdex 200 10/300 GL, GE Life Sciences) in HEK50G. Peak fractions were pooled, snap frozen in liquid nitrogen, and stored at −80°C.

Polymerization kinetics assays.

A Fluoromax-3 spectrofluorometer (Jobin Yvon, Inc) was used to monitor FtsZ polymerization by right-angle light scattering and tryptophan fluorescence. $FtsZ_1$ and/or $FtsZ_{AT}$ (wild-type or L71W/L72W mutants, as indicated in figures and text) was polymerized in HEK50 (50 mM HEPES-KOH pH 7.2, 50 mM KCl, 0.1 mM EDTA) with 2.5 mM $MgCl_2$. 2 mM GTP was used to induce polymerization for light scattering and 50 μM GTP was used to induce polymerization for tryptophan fluorescence (GTP is fluorescent at the wavelengths used, so low concentrations must be used). GTP was added after baseline light scatter or fluorescence was established. For light scattering, samples were excited at 350 nm and scatter was detected at 350 nm with slits set to 2 nm. For tryptophan fluorescence, samples were excited at 295 nm and emission was detected at 344 nm, with 2 nm slits.

GTPase assay.

$FtsZ_1$ and/or $FtsZ_{AT}$ was polymerized in HEK50 with 2.5 mM $MgCl_2$ and 2 mM GTP. GTP was added at time 0. Reaction was stopped at 5, 10, 15, 20, and 30 minutes with quench buffer (50 mM HEPES-KOH pH 7.2, 21.3 mM EDTA, 50 mM KCl). Inorganic phosphate in solution (liberated by GTP hydrolysis) over time was measured using SensoLyte MG Phosphate Assay Kit Colorimetric (AnaSpec, Inc, Fremont, California).

Negative stain transmission electron microscopy (TEM).

$FtsZ_1$ and/or $FtsZ_{AT}$ were polymerized in HEK50 with 2.5 mM $MgCl_2$ and 2 mM GTP. After a 15-minute incubation at room temperature, samples were applied to carbon-coated glow-discharged grids with 0.75% uranyl formate staining as previously described (Lariviere *et al.*, 2018, Sundararajan *et al.*, 2015). TEM samples were imaged using a Philips/FEI

BioTwin CM120 TEM equipped with an AMT XR80 8 megapixel CCD camera (AMT Imaging, USA).

Peptidoglycan composition analysis

Six cultures of WT and *ftsZ* depletion cells were grown in 10 ml of ATGN with IPTG to exponential phase. The 10 ml cell cultures were added to 40 ml of fresh media. The 50 ml cultures were grown to exponential phase and pelleted by centrifugation at 4000 x *g* for 10 minutes. Cell pellets were washed three times with ATGN by centrifugation and resuspension to remove IPTG. After the final wash 3 cell pellets were resuspended in 50 ml ATGN and the remaining 3 pellets were resuspended in 50 ml ATGN with 1 mM IPTG. Each culture was grown for 14 h. The optical densities of the cells were monitored to ensure the optical density of the cultures never went above OD_{600} = 0.7 to avoid changes to peptidoglycan content due to stationary phase. If necessary, fresh medium was added to dilute the cultures to maintain exponential growth. After 14 h of growth, 50 ml of the exponential cultures were collected and pelleted by centrifugation at 4000 x *g* for 20 minutes. Cell pellets were resuspended in 1mL of ATGN and 2 mL of 6% SDS and stirred with magnets while boiling for 4 h. After 4 h, samples were removed from heat but continued to stir overnight. Samples were then shipped to Dr. Felipe Cava's laboratory for purification and analysis.

Upon arrival, cells were boiled and simultaneously stirred by magnets for 2 h. After 2 h, boiling was stopped and samples were stirred overnight. Peptidoglycan was pelleted by centrifugation for 13 min at 60000 rpm (TLA100.3 Beckman rotor, Optima Max-TL ultracentrifuge; Beckman), and the pellets were washed 3 to 4 times by repeated cycles of centrifugation and resuspension in water. The pellet from the final wash was resuspended in 50 µl of 50 mM sodium phosphate buffer, pH 4.9, and digested overnight with 100 µg ml^{-1} of muramidase at 37°C. Muramidase digestion was stopped by boiling for 4 min. Coagulated protein was removed by centrifugation for 15 min at 15000 rpm in a desktop microcentrifuge. The muropeptides were mixed with 15 µl 0.5 M sodium borate and subjected to reduction of muramic acid residues into muramitol by sodium borohydride (10 mg ml^{-1} final concentration, 20 min at room temperature) treatment. Samples were adjusted to pH 3 to 4 with orthophosphoric acid and filtered (0.2-µm filters).

Muropeptides were analyzed on a Waters UPLC system equipped with an ACQUITY UPLC BEH C18 Column, 130 Å, 1.7 µm, 2.1 mm × 150 mm (Waters) and a dual wavelength absorbance detector. Elution of muropeptides was detected at 204 nm. Muropeptides were separated at 45°C using a linear gradient from buffer A [formic acid 0.1% (v/v)] to buffer B [formic acid 0.1% (v/v), acetonitrile 20% (v/v)] in a 12 min run with a 0.250 ml min^{-1} flow. Peptidoglycan compositional analysis on triplicate samples was completed on two separate occasions.

Supplementary Material

Refer to Web version on PubMed Central for supplementary material.

Acknowledgements

We thank Yves Brun from providing plasmids, Joe Lutkenhaus for providing *Escherichia coli* anti-FtsZ serum, and members of the Brown lab for helpful discussions and critical reading of this manuscript. PB and MH were supported by the National Science Foundation, IOS1557806. This work was funded in part by the National Institutes of Health through R01GM108640 (EDG) and T32GM007445 (training support of PJL). FC and AA receive funding support from Laboratory for Molecular Infection Medicine Sweden, Knut and Alice Wallenberg Foundation, Kempe and the Swedish Research Council. AA is supported by a MIMS/VR PhD position.

References

Aaron M, Charbon G, Lam H, Schwarz H, Vollmer W, and Jacobs-Wagner C (2007) The tubulin homologue FtsZ contributes to cell elongation by guiding cell wall precursor synthesis in *Caulobacter crescentus*. Mol Microbiol 64: 938–952. [PubMed: 17501919]

Aarsman ME, Piette A, Fraipont C, Vinkenvleugel TM, Nguyen-Disteche M, and den Blaauwen T (2005) Maturation of the *Escherichia coli* divisome occurs in two steps. Mol Microbiol 55: 1631–1645. [PubMed: 15752189]

Alvarez L, Hernandez SB, de Pedro MA, and Cava F (2016) Ultra-sensitive, high-resolution liquid chromatography methods for the high-throughput quantitative analysis of bacterial cell wall chemistry and structure. Methods in molecular biology (Clifton, N.J.) 1440: 11–27.

Bellefontaine AF, Pierreux CE, Mertens P, Vandenhaute J, Letesson JJ, and De Bolle X (2002) Plasticity of a transcriptional regulation network among alpha-proteobacteria is supported by the identification of CtrA targets in *Brucella abortus*. Mol Microbiol 43: 945–960. [PubMed: 11929544]

Bi EF, and Lutkenhaus J (1991) FtsZ ring structure associated with division in *Escherichia coli*. Nature 354: 161–164. [PubMed: 1944597]

Bisson-Filho AW, Hsu YP, Squyres GR, Kuru E, Wu F, Jukes C, Sun Y, Dekker C, Holden S, VanNieuwenhze MS, Brun YV, and Garner EC (2017) Treadmilling by FtsZ filaments drives peptidoglycan synthesis and bacterial cell division. Science (New York, N.Y.) 355: 739–743.

Botta GA, and Park JT (1981) Evidence for involvement of penicillin-binding protein 3 in murein synthesis during septation but not during cell elongation. Journal of bacteriology 145: 333–340. [PubMed: 6450748]

Brown PJB, de Pedro MA, Kysela DT, Van der Henst C, Kim J, De Bolle X, Fuqua C, and Brun YV (2012) Polar growth in the Alphaproteobacterial order Rhizobiales. Proceedings of the National Academy of Sciences of the United States of America 109: 1697–1701. [PubMed: 22307633]

Cameron TA, Anderson-Furgeson J, Zupan JR, Zik JJ, and Zambryski PC (2014) Peptidoglycan synthesis machinery in *Agrobacterium tumefaciens* during unipolar growth and cell division. mBio 5.

Cameron TA, Zupan JR, and Zambryski PC (2015) The essential features and modes of bacterial polar growth. Trends in Microbiology 23: 347–353. [PubMed: 25662291]

Chen Y, Bjornson K, Redick SD, and Erickson HP (2005) A rapid fluorescence assay for FtsZ assembly indicates cooperative assembly with a dimer nucleus. Biophysical journal 88: 505–514. [PubMed: 15475583]

Cheng J, Sibley CD, Zaheer R, and Finan TM (2007) A *Sinorhizobium meliloti* minE mutant has an altered morphology and exhibits defects in legume symbiosis. Microbiology (Reading, England) 153: 375–387.

Cho H, Wivagg CN, Kapoor M, Barry Z, Rohs PD, Suh H, Marto JA, Garner EC, and Bernhardt TG (2016) Bacterial cell wall biogenesis is mediated by SEDS and PBP polymerase families functioning semi-autonomously. Nature microbiology: 16172.

Curtis PD, and Brun YV (2014) Identification of essential alphaproteobacterial genes reveals operational variability in conserved developmental and cell cycle systems. Mol Microbiol 93: 713–735. [PubMed: 24975755]

de Boer P, Crossley R, and Rothfield L (1992) The essential bacterial cell-division protein FtsZ is a GTPase. Nature 359: 254–256. [PubMed: 1528268]

den Blaauwen T, Andreu JM, and Monasterio O (2014) Bacterial cell division proteins as antibiotic targets. Bioorganic chemistry 55: 27–38. [PubMed: 24755375]

Du S, and Lutkenhaus J (2017) Assembly and activation of the *Escherichia coli* divisome. Mol Microbiol 105: 177–187. [PubMed: 28419603]

Ducret A, Quardokus EM, and Brun YV (2016) MicrobeJ, a tool for high throughput bacterial cell detection and quantitative analysis. Nature microbiology 1: 16077.

Ehrle HM, Guidry JT, Iacovetto R, Salisbury AK, Sandidge DJ, and Bowman GR (2017) Polar organizing protein PopZ is required for chromosome segregation in *Agrobacterium* tumefaciens. Journal of bacteriology 199.

El-Kafafi el S, Mukherjee S, El-Shami M, Putaux JL, Block MA, Pignot-Paintrand I, Lerbs-Mache S, and Falconet D (2005) The plastid division proteins, FtsZ1 and FtsZ2, differ in their biochemical properties and sub-plastidial localization. The Biochemical journal 387: 669–676. [PubMed: 15601251]

Emami K, Guyet A, Kawai Y, Devi J, Wu LJ, Allenby N, Daniel RA, and Errington J (2017) RodA as the missing glycosyltransferase in *Bacillus subtilis* and antibiotic discovery for the peptidoglycan polymerase pathway. Nature microbiology 2: 16253.

Erickson HP, Anderson DE, and Osawa M (2010) FtsZ in bacterial cytokinesis: cytoskeleton and force generator all in one. Microbiology and molecular biology reviews : MMBR 74: 504–528. [PubMed: 21119015]

Figueroa-Cuilan W, Daniel JJ, Howell M, Sulaiman A, and Brown PJ (2016) Mini-Tn*7* Insertion in an artificial *att*Tn*7* site enables depletion of the essential master regulator CtrA in the phytopathogen *Agrobacterium* tumefaciens. Applied and environmental microbiology 82: 5015–5025. [PubMed: 27287320]

Figueroa-Cuilan WM, and Brown PJB (2018) Cell wall biogenesis during elongation and division in the plant pathogen *Agrobacterium tumefaciens*. Current topics in microbiology and immunology

Flores SA, Howell M, Daniel JJ, Piccolo R, and Brown PJB (2018) Absence of the Min system does not cause major cell division defects in *Agrobacterium tumefaciens*. Frontiers in microbiology 9: 681. [PubMed: 29686659]

Fraipont C, Alexeeva S, Wolf B, van der Ploeg R, Schloesser M, den Blaauwen T, and Nguyen-Disteche M (2011) The integral membrane FtsW protein and peptidoglycan synthase PBP3 form a subcomplex in *Escherichia coli*. Microbiology (Reading, England) 157: 251–259.

Fu G, Huang T, Buss J, Coltharp C, Hensel Z, and Xiao J (2010) In vivo structure of the E. coli FtsZ-ring revealed by photoactivated localization microscopy (PALM). PloS one 5: e12682.

Fujiwara T, and Fukui S (1974) Effect OF D-alanine and mitomycin-c on cell morphology of *Agrobacterium tumefaciens*. Gen App Microbiol 20: 345–349.

Goley ED, Dye NA, Werner JN, Gitai Z, and Shapiro L (2010) Imaging-based identification of a critical regulator of FtsZ protofilament curvature in *Caulobacter*. Molecular cell 39: 975–987. [PubMed: 20864042]

Goley ED, Yeh YC, Hong SH, Fero MJ, Abeliuk E, McAdams HH, and Shapiro L (2011) Assembly of the *Caulobacter* cell division machine. Mol Microbiol 80: 1680–1698. [PubMed: 21542856]

Goodner B, Hinkle G, Gattung S, Miller N, Blanchard M, Qurollo B, Goldman BS, Cao Y, Askenazi M, Halling C, Mullin L, Houmiel K, Gordon J, Vaudin M, Iartchouk O, Epp A, Liu F, Wollam C, Allinger M, Doughty D, Scott C, Lappas C, Markelz B, Flanagan C, Crowell C, Gurson J, Lomo C, Sear C, Strub G, Cielo C, and Slater S (2001) Genome sequence of the plant pathogen and biotechnology agent *Agrobacterium tumefaciens* C58. Science (New York, N.Y.) 294: 2323–2328.

Grangeon R, Zupan J, Jeon Y, and Zambryski PC (2017) Loss of PopZ At activity in Agrobacterium tumefaciens by Deletion or Depletion Leads to Multiple Growth Poles, Minicells, and Growth Defects. mBio 8.

Grangeon R, Zupan JR, Anderson-Furgeson J, and Zambryski PC (2015) PopZ identifies the new pole, and PodJ identifies the old pole during polar growth in *Agrobacterium tumefaciens*. Proceedings of the National Academy of Sciences of the United States of America 112: 11666–11671. [PubMed: 26324921]

Gray AN, Egan AJ, Van't Veer IL, Verheul J, Colavin A, Koumoutsi A, Biboy J, Altelaar AF, Damen MJ, Huang KC, Simorre JP, Breukink E, den Blaauwen T, Typas A, Gross CA, and Vollmer W (2015) Coordination of peptidoglycan synthesis and outer membrane constriction during *Escherichia coli* cell division. eLife 4.

Haeusser DP, and Levin PA (2008) The great divide: coordinating cell cycle events during bacterial growth and division. Current opinion in microbiology 11: 94–99. [PubMed: 18396093]

Haney SA, Glasfeld E, Hale C, Keeney D, He Z, and de Boer P (2001) Genetic analysis of the *Escherichia coli* FtsZ.ZipA interaction in the yeast two-hybrid system. Characterization of FtsZ residues essential for the interactions with ZipA and with FtsA. The Journal of biological chemistry 276: 11980–11987. [PubMed: 11278571]

Holden SJ, Pengo T, Meibom KL, Fernandez Fernandez C, Collier J, and Manley S (2014) High throughput 3D super-resolution microscopy reveals *Caulobacter crescentus* in vivo Z-ring organization. Proceedings of the National Academy of Sciences of the United States of America 111: 4566–4571. [PubMed: 24616530]

Howell M, Aliashkevich A, Salisbury AK, Cava F, Bowman GR, and Brown PJB (2017a) Absence of the polar organizing protein PopZ results in reduced and asymmetric cell division in *Agrobacterium tumefaciens*. Journal of bacteriology 199.

Howell M, and Brown PJB (2016) Building the bacterial cell wall at the pole. Current opinion in microbiology 34: 53–59. [PubMed: 27504539]

Howell M, Daniel J, and J.B. Brown P, (2017b) Live cell fluorescence microscopy to observe essential processes during microbial cell growth. J Vis Exp

Kuru E, Velocity Hughes H, Brown PJ, Hall E, Tekkam S, Cava F, de Pedro MA, Brun YV, and VanNieuwenhze MS (2012) *In situ* probing of newly synthesized peptidoglycan in live bacteria with fluorescent D-amino acids. Angewandte Chemie (International ed. in English) 51: 12519–12523. [PubMed: 23055266]

Lariviere PJ, Szwedziak P, Mahone CR, Lowe J, and Goley ED (2018) FzlA, an essential regulator of FtsZ filament curvature, controls constriction rate during *Caulobacter* division. Mol Microbiol 107: 180–197. [PubMed: 29119622]

Latch JN, and Margolin W (1997) Generation of buds, swellings, and branches instead of filaments after blocking the cell cycle of *Rhizobium meliloti*. Journal of bacteriology 179: 2373–2381. [PubMed: 9079925]

Li Z, Trimble MJ, Brun YV, and Jensen GJ (2007) The structure of FtsZ filaments in vivo suggests a force-generating role in cell division. The EMBO journal 26: 4694–4708. [PubMed: 17948052]

Ma X, and Margolin W (1999) Genetic and functional analyses of the conserved C-terminal core domain of *Escherichia coli* FtsZ. Journal of bacteriology 181: 7531–7544. [PubMed: 10601211]

Margolin W, and Long SR (1994) *Rhizobium meliloti* contains a novel second homolog of the cell division gene ftsZ. Journal of bacteriology 176: 2033–2043. [PubMed: 8144471]

Meeske AJ, Riley EP, Robins WP, Uehara T, Mekalanos JJ, Kahne D, Walker S, Kruse AC, Bernhardt TG, and Rudner DZ (2016) SEDS proteins are a widespread family of bacterial cell wall polymerases. Nature 537: 634–638. [PubMed: 27525505]

Meier EL, and Goley ED (2014) Form and function of the bacterial cytokinetic ring. Current opinion in cell biology 26: 19–27. [PubMed: 24529242]

Meier EL, Razavi S, Inoue T, and Goley ED (2016) A novel membrane anchor for FtsZ is linked to cell wall hydrolysis in *Caulobacter crescentus*. Mol Microbiol 101: 265–280. [PubMed: 27028265]

Moll A, and Thanbichler M (2009) FtsN-like proteins are conserved components of the cell division machinery in proteobacteria. Mol Microbiol 72: 1037–1053. [PubMed: 19400794]

Monahan LG, Hajduk IV, Blaber SP, Charles IG, and Harry EJ (2014) Coordinating bacterial cell division with nutrient availability: a role for glycolysis. mBio 5: e00935–00914. [PubMed: 24825009]

Morton ER, and Fuqua C (2012a) Laboratory maintenance of Agrobacterium. Current protocols in microbiology Chapter 1: Unit3D 1.

Morton ER, and Fuqua C (2012b) Unit 3D.2 genetic manipulation of Agrobacterium. Current protocols in microbiology Chapter: Unit-3D.2.

Mosyak L, Zhang Y, Glasfeld E, Haney S, Stahl M, Seehra J, and Somers WS (2000) The bacterial cell-division protein ZipA and its interaction with an FtsZ fragment revealed by X-ray crystallography. The EMBO journal 19: 3179–3191. [PubMed: 10880432]

Muller FD, Raschdorf O, Nudelman H, Messerer M, Katzmann E, Plitzko JM, Zarivach R, and Schuler D (2014) The FtsZ-like protein FtsZm of *Magnetospirillum gryphiswaldense* likely interacts with

its generic homolog and is required for biomineralization under nitrate deprivation. Journal of bacteriology 196: 650–659. [PubMed: 24272781]

Olson BJ, Wang Q, and Osteryoung KW (2010) GTP-dependent heteropolymer formation and bundling of chloroplast FtsZ1 and FtsZ2. The Journal of biological chemistry 285: 20634–20643. [PubMed: 20421292]

Ortiz C, Natale P, Cueto L, and Vicente M (2016) The keepers of the ring: regulators of FtsZ assembly. FEMS microbiology reviews 40: 57–67. [PubMed: 26377318]

Pichoff S, and Lutkenhaus J (2007) Identification of a region of FtsA required for interaction with FtsZ. Mol Microbiol 64: 1129–1138. [PubMed: 17501933]

Pini F, De Nisco NJ, Ferri L, Penterman J, Fioravanti A, Brilli M, Mengoni A, Bazzicalupo M, Viollier PH, Walker GC, and Biondi EG (2015) Cell cycle control by the master regulator CtrA in *Sinorhizobium meliloti*. PLOS Genetics 11: e1005232. [PubMed: 25978424]

Pini F, Frage B, Ferri L, De Nisco NJ, Mohapatra SS, Taddei L, Fioravanti A, Dewitte F, Galardini M, Brilli M, Villeret V, Bazzicalupo M, Mengoni A, Walker GC, Becker A, and Biondi EG (2013) The DivJ, CbrA and PleC system controls DivK phosphorylation and symbiosis in *Sinorhizobium meliloti*. Mol Microbiol 90: 54–71. [PubMed: 23909720]

Richards DM, Hempel AM, Flardh K, Buttner MJ, and Howard M (2012) Mechanistic basis of branch-site selection in filamentous bacteria. PLoS computational biology 8: e1002423. [PubMed: 22423220]

Rowlett VW, and Margolin W (2015) The Min system and other nucleoid-independent regulators of Z ring positioning. Frontiers in microbiology 6: 478. [PubMed: 26029202]

Sundararajan K, Miguel A, Desmarais SM, Meier EL, Huang KC, and Goley ED (2015) The bacterial tubulin FtsZ requires its intrinsically disordered linker to direct robust cell wall construction. Nature communications 6: 7281.

Szwedziak P, Wang Q, Freund SM, and Lowe J (2012) FtsA forms actin-like protofilaments. The EMBO journal 31: 2249–2260. [PubMed: 22473211]

TerBush AD, MacCready JS, Chen C, Ducat DC, and Osteryoung KW (2018) Conserved dynamics of chloroplast cytoskeletal FtsZ proteins across photosynthetic lineages. Plant physiology 176: 295–306. [PubMed: 28814573]

Varma A, and Young KD (2004) FtsZ collaborates with penicillin binding proteins to generate bacterial cell shape in *Escherichia coli*. Journal of bacteriology 186: 6768–6774. [PubMed: 15466028]

Vaughan S, Wickstead B, Gull K, and Addinall SG (2004) Molecular evolution of FtsZ protein sequences encoded within the genomes of archaea, bacteria, and eukaryota. Journal of molecular evolution 58: 19–29. [PubMed: 14743312]

Ward JE Jr., and Lutkenhaus J (1985) Overproduction of FtsZ induces minicell formation in *E. coli*. Cell 42: 941–949. [PubMed: 2996784]

Wood DW, Setubal JC, Kaul R, Monks DE, Kitajima JP, Okura VK, Zhou Y, Chen L, Wood GE, Almeida NF Jr., Woo L, Chen Y, Paulsen IT, Eisen JA, Karp PD, Bovee D Sr., Chapman P, Clendenning J, Deatherage G, Gillet W, Grant C, Kutyavin T, Levy R, Li MJ, McClelland E, Palmieri A, Raymond C, Rouse G, Saenphimmachak C, Wu Z, Romero P, Gordon D, Zhang S, Yoo H, Tao Y, Biddle P, Jung M, Krespan W, Perry M, Gordon-Kamm B, Liao L, Kim S, Hendrick C, Zhao ZY, Dolan M, Chumley F, Tingey SV, Tomb JF, Gordon MP, Olson MV, and Nester EW (2001) The genome of the natural genetic engineer *Agrobacterium tumefaciens* C58. Science (New York, N.Y.) 294: 2317–2323.

Wu LJ, and Errington J (2004) Coordination of cell division and chromosome segregation by a nucleoid occlusion protein in *Bacillus subtilis*. Cell 117: 915–925. [PubMed: 15210112]

Yang X, Lyu Z, Miguel A, McQuillen R, Huang KC, and Xiao J (2017) GTPase activity-coupled treadmilling of the bacterial tubulin FtsZ organizes septal cell wall synthesis. Science (New York, N.Y.) 355: 744–747.

Zupan JR, Cameron TA, Anderson-Furgeson J, and Zambryski PC (2013) Dynamic FtsA and FtsZ localization and outer membrane alterations during polar growth and cell division in *Agrobacterium tumefaciens*. Proceedings of the National Academy of Sciences of the United States of America 110: 9060–9065. [PubMed: 23674672]

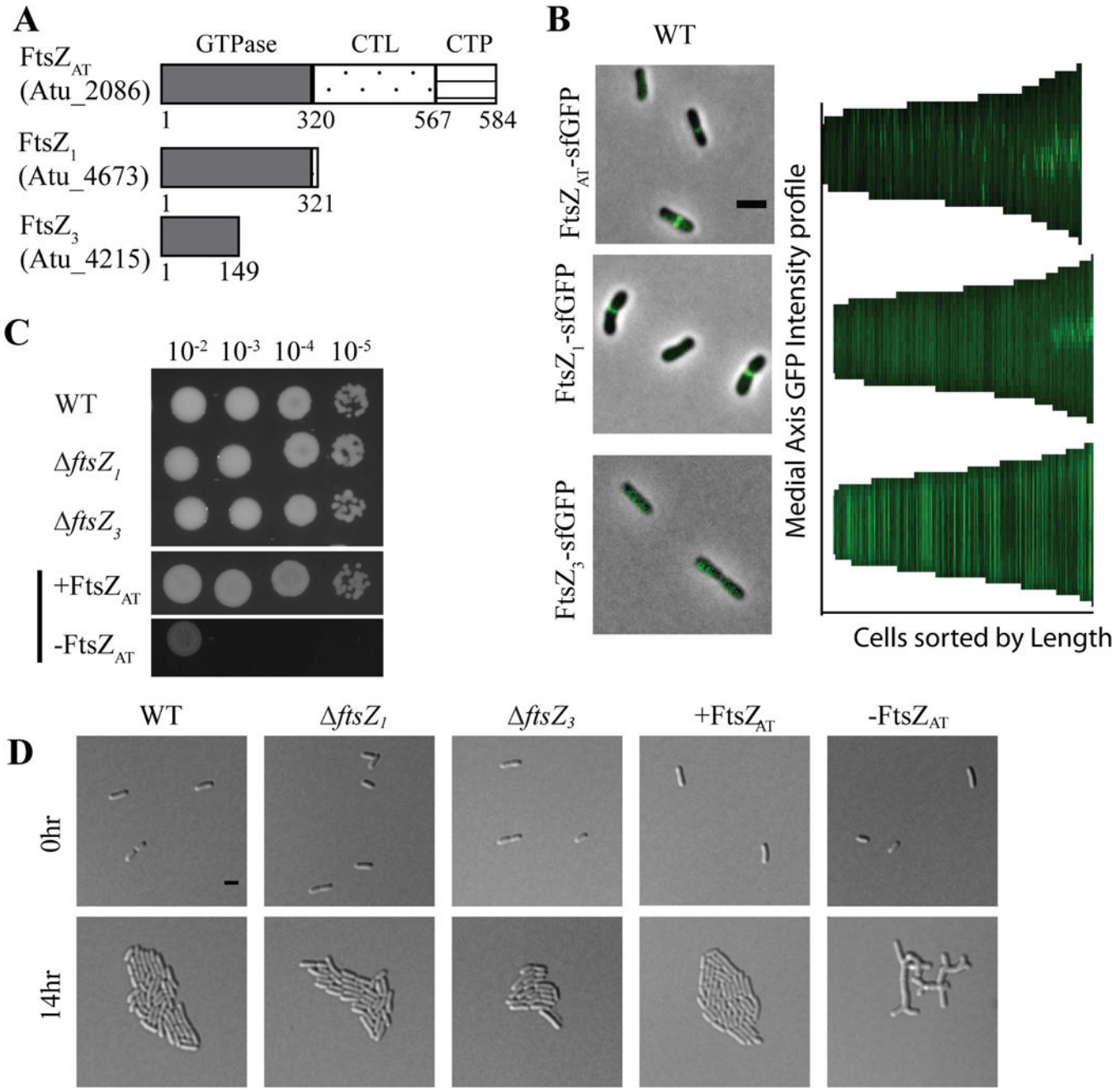

Figure 1. Characterization of FtsZ homologs in *A. tumefaciens*.

A) Domain schematic of FtsZ homologs in *A. tumefaciens*. Note that domains are not drawn to scale. B) Representative image of localization patterns for each FtsZ homolog expressed in wildtype cells. Demographs depict localization of FtsZ homologs at a population level. Median profiles of the GFP channel of 225–240 cells per strain are stacked and ordered by cell length. C) Cell viability is shown by spotting serial dilutions. (+$FtsZ_{AT}$ is spotted on ATGN with IPTG while all other strains are spotted on ATGN without IPTG). D) Cell morphology and microcolony formation are shown for WT, Δ*ftsZ*$_1$ and Δ*ftsZ*$_3$, and the

ftsZ$_{AT}$ depletion strain under induced (+FtsZ$_{AT}$) and uninduced (-FtsZ$_{AT}$) conditions. All scale bars are set to 2 μm.

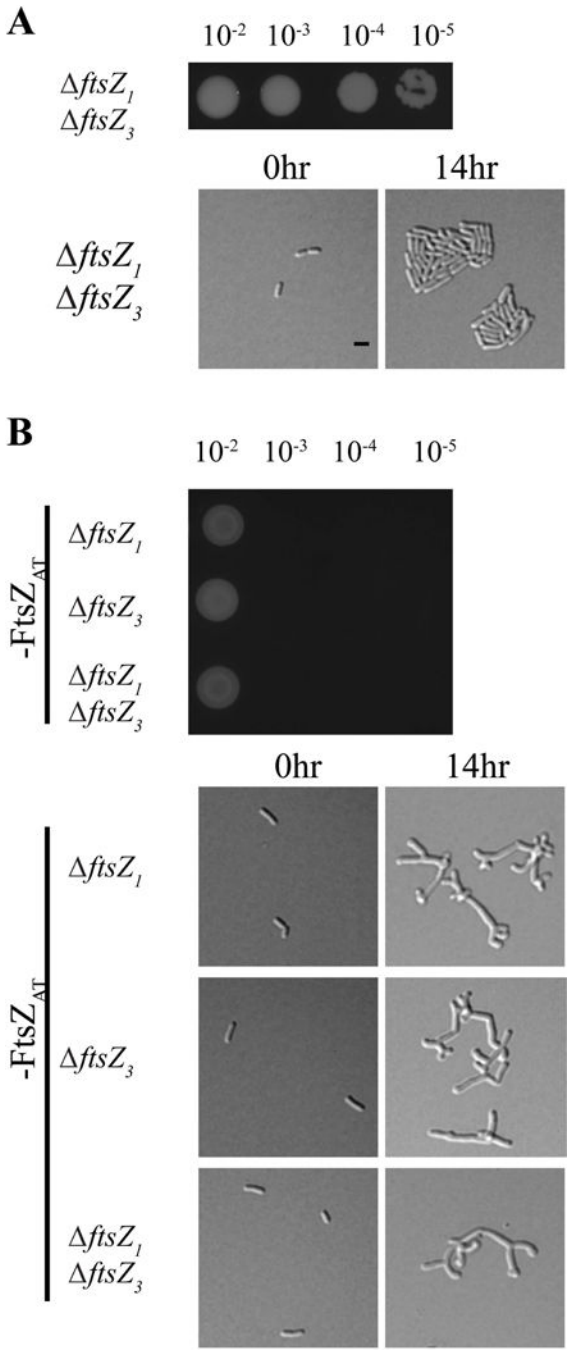

Figure 2. Removal of additional *ftsZ* homologs in the *ftsZ$_{AT}$* depletion strain does not cause a more severe phenotype.

A) Cell viability (top) and morphology (bottom) of the double mutant Δ*ftsZ$_1$*Δ*ftsZ$_3$*. B) Cell viability (top) and morphology (bottom) of Δ*ftsZ$_1$*, Δ*ftsZ$_3$*, or Δ*ftsZ$_1$*Δ*ftsZ$_3$* during $FtsZ_{AT}$ depletion. All scale bars are set to 2 μm. Black bar denotes *ftsZ$_{AT}$* depletion strain background.

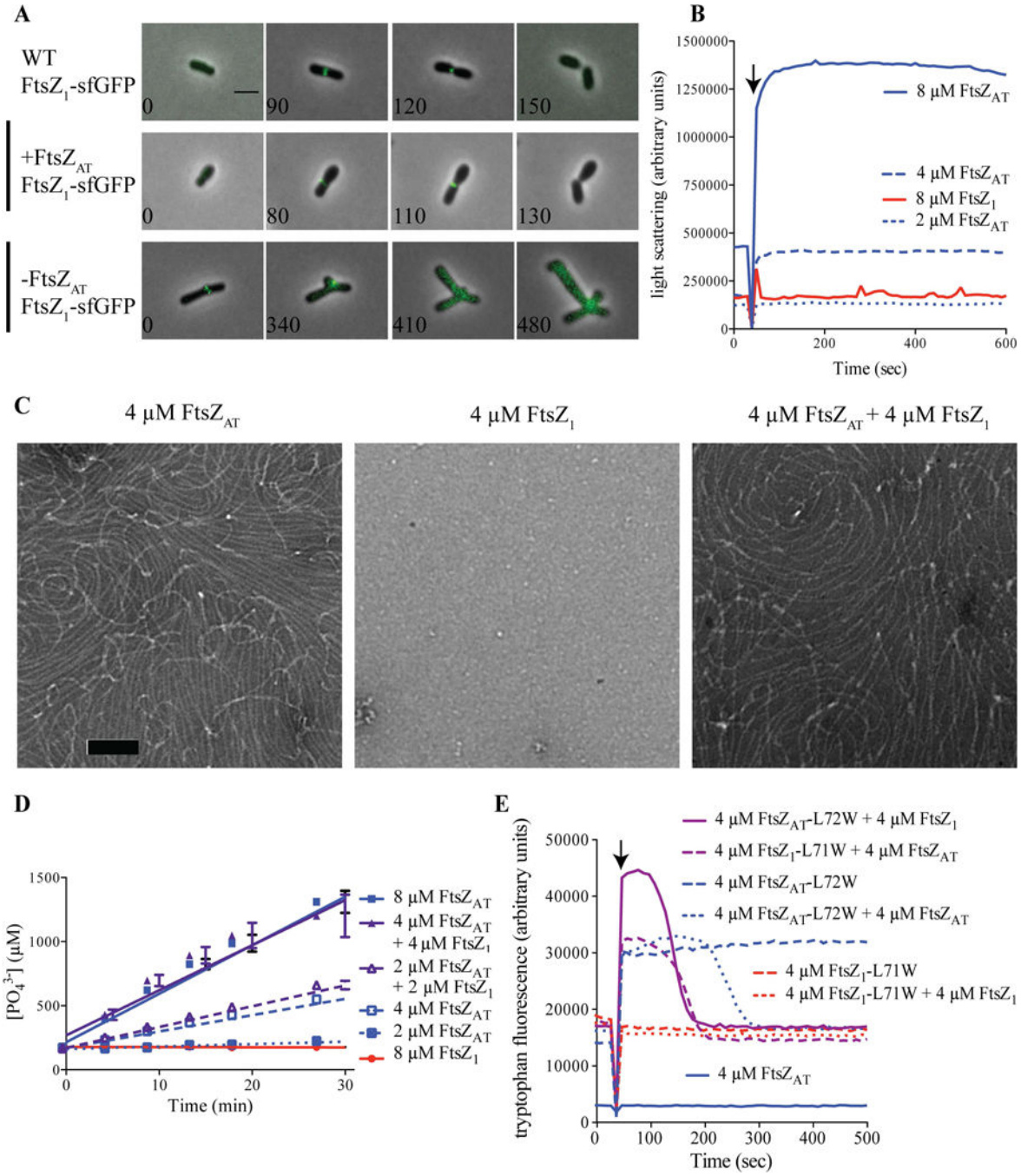

Fgure 3. FtsZ$_1$ requires FtsZ$_{AT}$ to polymerize *in vitro* and to localize in cells.

A) FtsZ$_1$-sfGFP localization in WT, +FtsZ$_{AT}$ and -FtsZ$_{AT}$. Scale bar is set to 2 μm. B) Light scattering over time for purified proteins at the indicated concentrations. GTP (2 mM) was added where indicated by the arrow to induce polymerization. Experiments were performed in triplicate and mean curves are shown. C) Negative stain TEM of the indicated proteins. Co-polymers of FtsZ$_{AT}$ and FtsZ$_1$ are indistinguishable from FtsZ$_{AT}$ polymers. Scale bar is set to 100 nm. D) Inorganic phosphate concentration in solution over time in the presence of the indicated proteins and protein concentrations. Reactions were performed in triplicate and

mean ± standard error is plotted. E) Tryptophan fluorescence over time for the indicated proteins. $FtsZ_1$-L71W (red) shows no polymerization (Trp fluorescence) on its own, but can co-polymerize with added $FtsZ_{AT}$ (purple). GTP (50 μM) was added where indicated by the arrow to induce polymerization. Experiments were performed in triplicate and representative curves are shown.

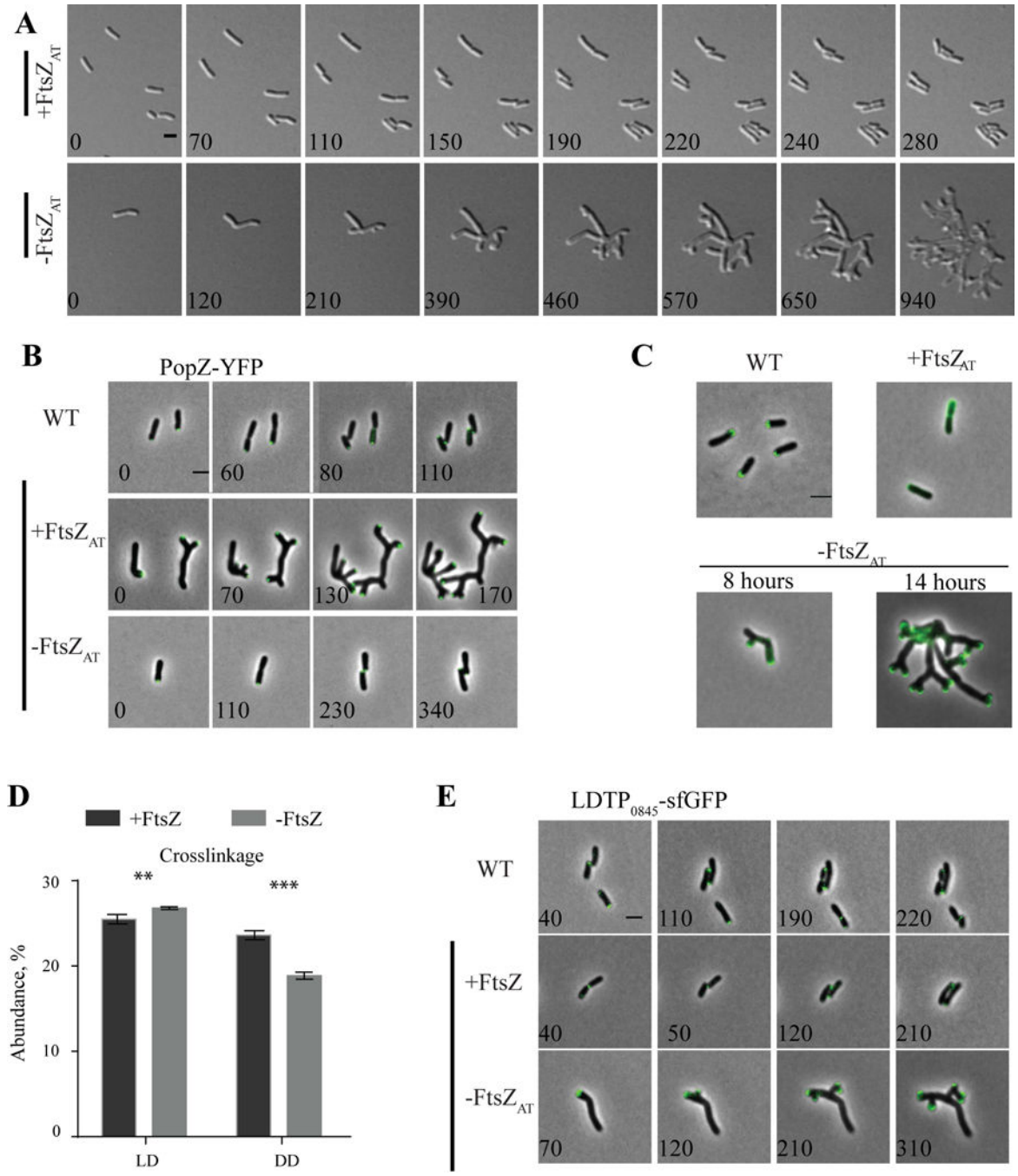

Figure 4. Characterization of continuous polar growth during FtsZ$_{AT}$ depletion.

A) Timelapse microscopy of the *ftsZ$_{AT}$* depletion strain under inducing conditions (+FtsZ$_{AT}$, top panel) and depletion conditions (-FtsZ$_{AT}$, bottom panel). B) Timelapse microscopy showing PopZ-YFP localization WT, +FtsZ$_{AT}$ and -FtsZ$_{AT}$. C) FDAA labeling of WT cells, and cells depleted of FtsZ$_{AT}$ for 0 hours (+FtsZ$_{AT}$), 8 hours, and 14 hours. D) Abundance of total LD and DD crosslinkage in peptidoglycan isolated from *ftsZ$_{AT}$* depletion strain after induction (+FtsZ$_{AT}$, black bars) or depletion (-FtsZ$_{AT}$, grey bars) of FtsZ$_{AT}$ for 14 hours. Data shown are the average abundance of each crosslinkage type and are taken from analysis

of three independent biological samples. Statistical significance was calculated by t-tests and is indicated with an asterisk (P-value <0.05 (*), <0.005 (**), <0.001 (***)). E) Timelapse microscopy of $LDTP_{0845}$-sfGFP in WT, $+FtsZ_{AT}$ and $-FtsZ_{AT}$ a. All scale bars are set to 2 μm.

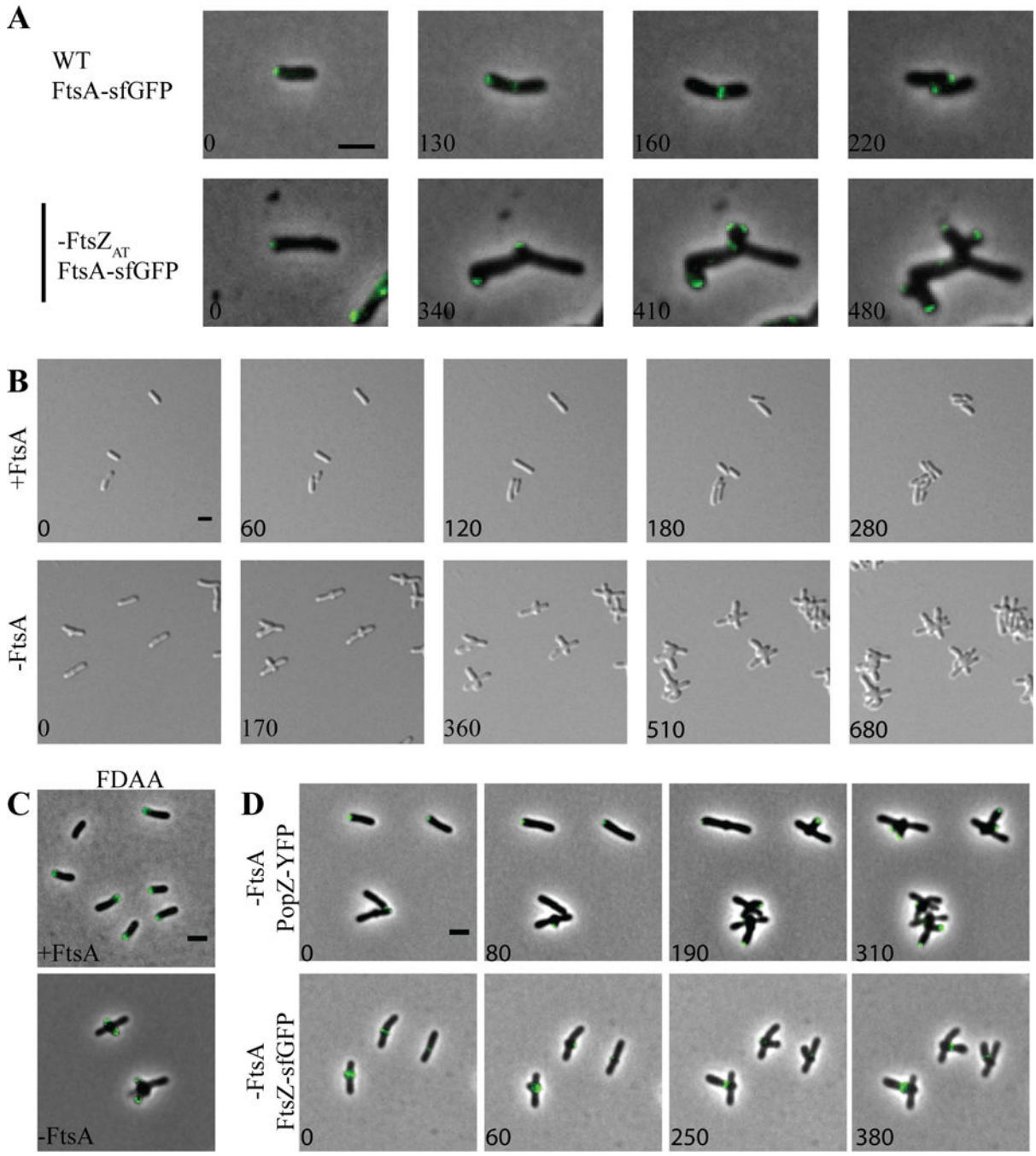

Figure 5. FtsA is not required for initiation of mid-cell growth.

A) FtsA-sfGFP localization in WT (top panel) and cells depleted of $FtsZ_{AT}$ (bottom panel). B) Timelapse microscopy shows typical morphology when FtsA is induced and morphological changes in the absence of FtsA. C) FDAA labeling of the *ftsA* depletion strain after 8 hours of induction (+FtsA) or depletion (-FtsA). D) Timelapse microscopy of PopZ-YFP localization (top) and $FtsZ_{AT}$-GFP localization (bottom) during FtsA depletion. All scale bars are set to 2 μm.

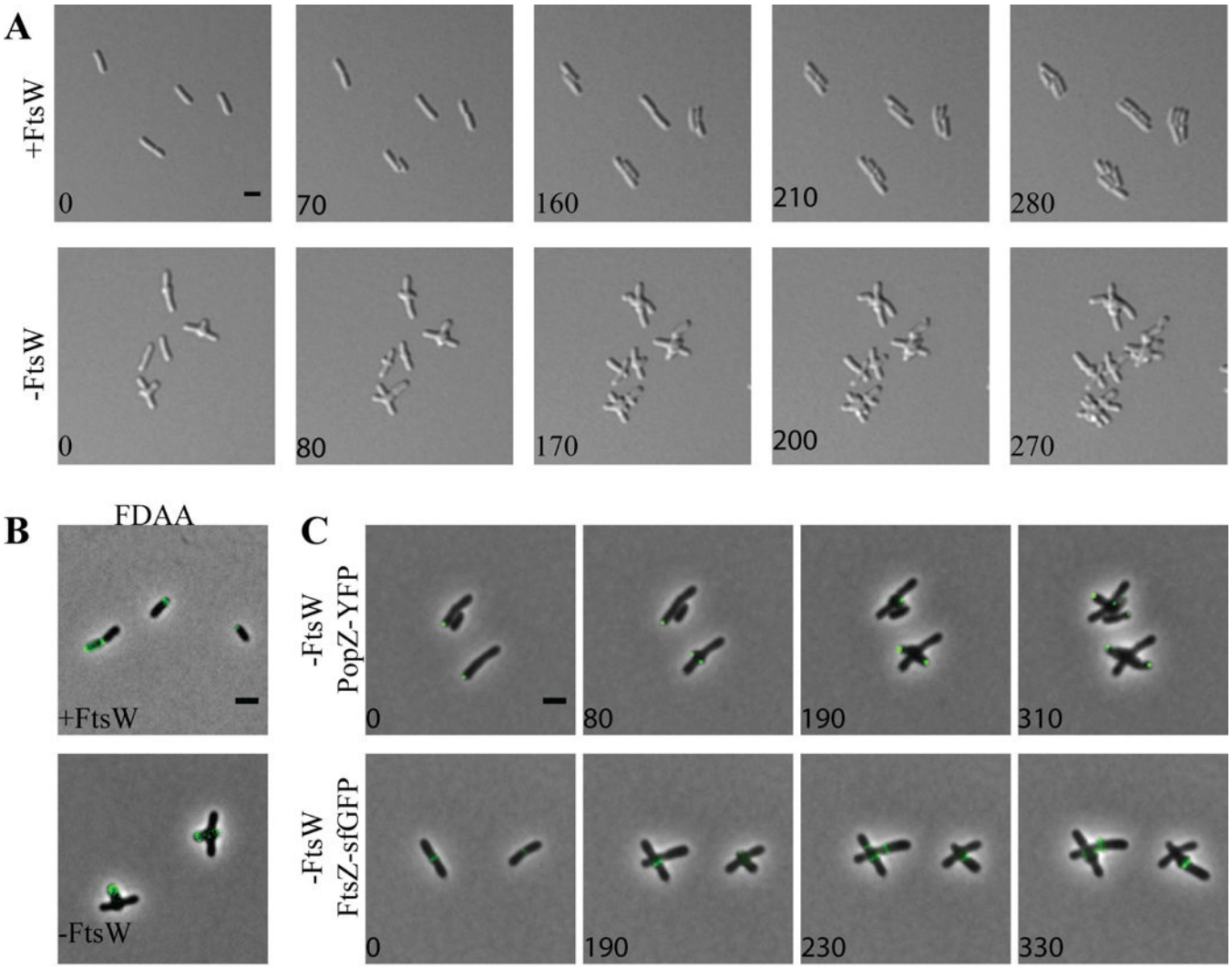

Figure 6. FtsW is not required for initiation of mid-cell growth

A) Timelapse microscopy of the *ftsW* depletion strain when induced (+FtsW, top) or depleted (-FtsWm bottom). B) FDAA labeling of the *ftsW* depletion strain after 8 hours of induction (+FtsW) or depletion (-FtsW). C) Timelapse microscopy of PopZ-YFP localization (top) and $FtsZ_{AT}$-GFP localization (bottom) during FtsW depletion. All scale bars are set to 2 μm.

Table 1.

Quantitation of cell size and constriction of *ftsZ* mutants

		Average Cell Length[†] (μm +/− SD[‡])	Average Cell Area[†] (μm^2 +/− SD)	Average Constriction Rate[‡] (nm/min +/− SD)	Relative Constriction Position[§] +/− SD
WT		2.31 +/−.50	1.66 +/−.35	6.82 +/−3.19	.49 +/−.05
ΔftsZ$_1$		2.25 +/−.49	1.52 +/−.33	6.99 +/−3.58	.46 +/−.05
ΔftsZ$_3$		2.24 +/−.47	1.44 +/−.30	6.77 +/−2.77	.46 +/−.05
ΔftsZ$_1$ ΔftsZ$_3$		2.25 +/−.51	1.47 +/−.34	6.61 +/−3.75	.46 +/−.04
ftsZ$_{AT}$ depletion	-FtsZ$_{AT}$ 0 h	2.71 +/−.70	1.56 +/−.39	6.38 +/−2.81	.49 +/−.07
	-FtsZ$_{AT}$ 8 h	ND[¶]	2.95 +/−1.12	ND	ND
	-FtsZ$_{AT}$ 14 h	ND	11.37 +/−4.69	ND	ND

[†]At least 100 cells were used to quantify the cell length and area for each strain.

[‡]At least 30 cells were used to quantify the constriction rates for each strain.

[§]Relative constriction position for at least 40 cells is shown. A value of 0 corresponds to the new pole, 0.5 corresponds to mid-cell, and a value of 1 corresponds to the old pole.

[¶]ND – not determined.

Table 2.

Quantitation of growth active and inactive poles and cell area

		Average Number Growth Inactive Poles† ±SD	Average Number Growth Active Poles† ±SD	Average Cell Area† (μm² +/− SD)
ftsZ$_{AT}$ depletion	-FtsZ$_{AT}$ 14 h	1.19 ±0.41	7.36 ±2.76	11.37 ±4.69
	-FtsZ$_{AT}$ 14 h Δ*ftsZ1*	1.14 ±0.38	7.22 ±2.77	10.89 ±3.25
	-FtsZ$_{AT}$ 14 h Δ*ftsZ3*	1.16 ±0.42	7.10 ±2.89	11.12 ±5.61
	-FtsZ$_{AT}$ 14 h Δ*ftsZ1* Δ*ftsZ3*	1.14 ±0.41	7.14 ±2.71	10.34 ± 4.27

† 100 cells were used to quantify the number of growth active and inactive poles and cell area in each strain.